SHiP
Search for Hidden Particles

CERN-SHiP-NOTE-2019-003
June 5, 2020

Measurement of the muon flux for the SHiP experiment

C. Ahdida[12], A. Akmete[16], A. Bay[14], D. Bick[3], S. Bieschke[3], W.M. Bonivento[5], A. Buonaura[15], M. Campanelli[18], M. Casolino[12], N. Charitonidis[12], M. Cristinziani[2], A. Crupano[6,b], R. de Asmundis[6], G. De Lellis[6,9,12,b], M. De Serio[4,a], A. Di Crescenzo[6,b], H. Dijkstra[12], O. Durhan[16], E. Elikkaya[16], R. Froeschl[12], F. Fedotov[18], A. Golutvin[17,9], P. Gorbounov[12], M. Gorshenkov[9], A.L. Grandchamp[14], G.J. Haefeli[14], E. van Herwijnen[12], M. Hushchyn[11], A. Iuliano[6,b], R. Jacobsson[12], M. Jonker[12], E. Khalikov[10], N. Konovalova[8,9], A. Korzenev[13], V. Kostyukhin[2], O. Lantwin[15], P. Mermod[13], N. Okateva[8,9], B. Opitz[3], N. Owtscharenko[2], A. Pastore[4], F. Redi[14], A.B. Rodrigues Cavalcante[14], T. Ruf[12], A. Shakin[9], S. Shirobokov[17], S. Simone[4,a], M.E. Stramaglia[14], D. Sukhonos[12], V. Tioukov[6], G. Vankova-Kirilova[1], N. Wojcicka[12], C.S. Yoon[7]

Abstract

We report the results of the measurement of the muon flux emanating from the SHiP target at the CERN SPS. A replica of the SHiP target followed by a 2.4 m iron hadron absorber was installed in the H4 400 GeV/c proton beamline. To measure the momentum spectrum, a spectrometer consisting of drift tubes and resistive plate chambers (RPCs) was placed around the Goliath magnet. During a three week period a dataset for analysis corresponding to 3.25×10^{11} protons on target (POT) was recorded. This amounts to approximatively 1% of a SHiP spill. The amount of accumulated data allows us to make a validation of the results from our Pythia and Geant4 based Monte Carlo (FairShip).

[1] *Faculty of Physics, Sofia University, Sofia, Bulgaria*
[2] *Physikalisches Institut, Universität Bonn, Bonn, Germany*
[3] *Universität Hamburg, Hamburg, Germany*
[4] *Sezione INFN di Bari, Bari, Italy*
[5] *Sezione INFN di Cagliari, Cagliari, Italy*
[6] *Sezione INFN di Napoli, Napoli, Italy*
[7] *Physics Education Department & RINS, Gyeongsang National University, Jinju, Korea*
[8] *P.N. Lebedev Physical Institute (LPI), Moscow, Russia*
[9] *National University of Science and Technology "MISiS", Moscow, Russia*
[10] *Skobeltsyn Institute of Nuclear Physics of Moscow State University (SINP MSU), Moscow, Russia*
[11] *Yandex School of Data Analysis, Moscow, Russia*
[12] *European Organization for Nuclear Research (CERN), Geneva, Switzerland*
[13] *University of Geneva, Geneva, Switzerland*
[14] *École Polytechnique Fédérale de Lausanne (EPFL), Lausanne, Switzerland*
[15] *Physik-Institut, Universität Zürich, Zürich, Switzerland*
[16] *Middle East Technical University (METU), Ankara, Turkey*

[17] *Imperial College London, London, United Kingdom*
[18] *University College London, London, United Kingdom*
[a] *Università di Bari, Bari, Italy*
[b] *Università di Napoli "Federico II", Napoli, Italy*

VERSION	DATE	COMMENTS
01	18.03.2019	First version
02	12.09.2019	Second version - before meeting 24.09.2019
03	02.10.2019	Third version - with ghost section and corrected target position in MC
04	02.10.2019	Fourth version - included some forgotten comments
05	24.10.2019	Fifth version - after meetings 08.10.2019/22.10.2019
05-01	1.11.2019	minor update to track efficiency with zero field
06	25.11.2019	after RT correction, refitted data, 350mu MC
07	03.12.2019	after meeting 03.12.2019
08	14.05.2020	adding inactive RPC channels to MC simulation†

† During the J/ψ cross section analysis, it had been found out that the muflux MC simulation does not reproduce the RPC dead channels. This leads to an overestimate of the MC acceptance for tracks below 25 GeV/c. This has been corrected, the affected plots and tables have been redone.

Contents

1 Motivation and experimental setup **1**

2 Alignment from survey **2**

3 Magnetic field **2**

4 Data **4**

5 Normalization **4**

6 Calibration **5**
6.1 Drift tube r-t calibration 5
6.2 Alignment and hit resolution 8

7 Reconstruction **11**
7.1 Drift tube pattern recognition 11
7.2 RPC pattern recognition 11
7.3 Track fitting 12
7.4 Clone removal 12
7.5 Momentum resolution 12
7.6 Effect of degraded drift tube resolution 13

8 Ghost tracks **14**

9 Data quality monitoring **15**

10 Reconstruction efficiencies **15**
10.1 Drift tube hit efficiencies using fitted tracks 16
10.2 Drift tube hit efficiencies using RPC tracks 19
10.3 Tracking efficiency in data 20
10.4 Tracking efficiency in MC 22
10.4.1 Delta rays 24
10.5 RPC detector efficiency 25

11 Comparison with Monte Carlo data **29**

12 Results **30**

13 Conclusions **31**

1 Motivation and experimental setup

A major concern for the design of the SHiP experiment [1] is the lack of a precise knowledge of the muon flux and its momentum spectrum. Therefore the SHiP Collaboration proposed to measure the expected muon flux in the experiment by installing a cylindrical replica (10 cm diameter and 154.3 cm length) of the SHiP target in a 400 GeV/c proton beam at the H4 beam line of the SPS at CERN [2] in July 2018.

The muon flux spectrometer, as implemented in FairShip (the SHiP software framework), is shown in Figure 1. The target was followed by a hadron absorber made of iron blocks

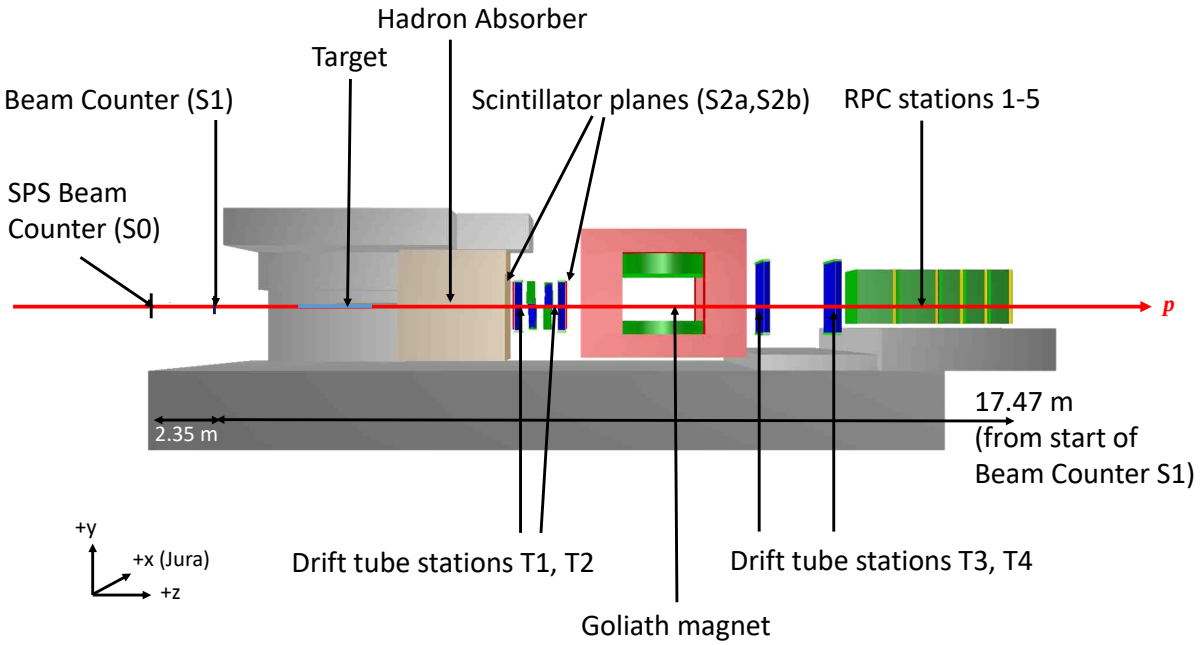

Figure 1: Layout of the spectrometer to measure the μ-flux. The FairShip coordinate system is also shown.

($240 \times 240 \times 240$ cm^3) and surrounded by iron and concrete shielding blocks. The dimensions of the hadron absorber were chosen to stop pions and kaons but to keep a good p_T acceptance of traversing muons.[1]

The SPS beam counters (XSCI.022.480/481, S0 in Figure 1) are 10×10 cm^2 scintillators. Its discriminator produces a 20 ns wide signal, which is counted in scaler SC00. A beam counter scintillator (S1) was placed in front of the target shielding. S1 consists of two 16×16 mm^2 scintillators. Each scintillator is viewed by two photomultipliers (PMs).

[1] MC origin of reconstructed tracks per 10^6 POT:

$E_{kin} > E_{min}$	e^-	K^+	K^-	p	π^-	π^+	μ^-	μ^+
1 GeV/c	0.00	0.06	0.06	0.28	0.56	0.89	378.89	443.11
10 GeV/c	0.00	0.06	0.00	0.00	0.06	0.5	153.17	184.11

Their discriminators produce a 30 ns wide signal, which is recorded in time to digital converters (TDCs). The four discriminating signals are required to be in coincidence, and this coincidence signal (S1-coincidence) is counted in scaler SC01.

Downstream of the hadron absorber there were four drift tube tracking stations (T1-T4, modified from the OPERA experiment [3]), two placed upstream of the Goliath magnet and two downstream. The scintillators S2 consist of two 55×110 cm^2 scintillators, placed before (S2a) and behind (S2b) the first two tracking stations. Each scintillator is viewed by two PMs. Their discriminators produce a 50 ns wide signal, and they are recorded in TDCs.

Muon candidates are identified by S2 by requiring a coincidence of 2 out of the 4 photomultipliers. The data acquisition is triggered by the $(\mathrm{S1-coincidence}) \wedge (\mathrm{S2-coincidence})$.

The drift tubes are arranged in modules of 48 tubes, staggered in four layers of twelve tubes with a total width of approximately 50 cm. The four modules of height 110 cm making up stations T1 and T2 were arranged in a stereo setup ($x-u$ views for T1 and $x-y$ views for T2), with a stereo angle of 60°. T3 and T4 had only x views and are made of four modules of 160 cm height.

A muon tagger was placed behind the two downstream drift tube stations. It consisted of 5 planes of Resistive Plate Chambers (RPCs) interleaved with 1×80 cm and 3×40 cm thick iron slabs. In addition to this, a 80 cm thick iron slab was positioned immediately upstream of the first chamber. The active area of the RPCs was 190 cm $\times$ 120 cm and each chamber was readout by two panels of X/Y strips with a 1 cm pitch.

The two upstream tracking stations were centered on the beam line, whereas the two downstream stations and the RPCs were centered on the Goliath opening to maximize the acceptance.

The protons were delivered in 4.8 s duration spills (slow extraction). There were either one or two spills per SPS supercycle, with intensities between 10^6 and 10^7 protons per spill. 1 sigma of the beam spot was 2 mm.

2 Alignment from survey

The experimental setup of the muon flux spectrometer was aligned by the CERN survey team. The analysis of their results and the implementation in FairShip has been described in [4]. The precision of this initial alignment was ~ 0.5 mm.

3 Magnetic field

The magnetic field of the Goliath magnet was measured by the CERN EN-EA and EP-DT groups [5]. The measurements were taken in the volume $-72 < x < 84$ cm, $-23 < y < 59$ cm and $-176 < z < 184$ cm. However, as the measured field-map does not fill the entire Goliath aperture, the y component of the magnetic field ($\mathrm{B_y}$) was extended by extrapolation to the area $-114 < x < 126$ cm, $-44 < y < 80$ cm and

$-254 < z < 256$ cm. This is shown in Figure 2. The Goliath magnet is powered by two

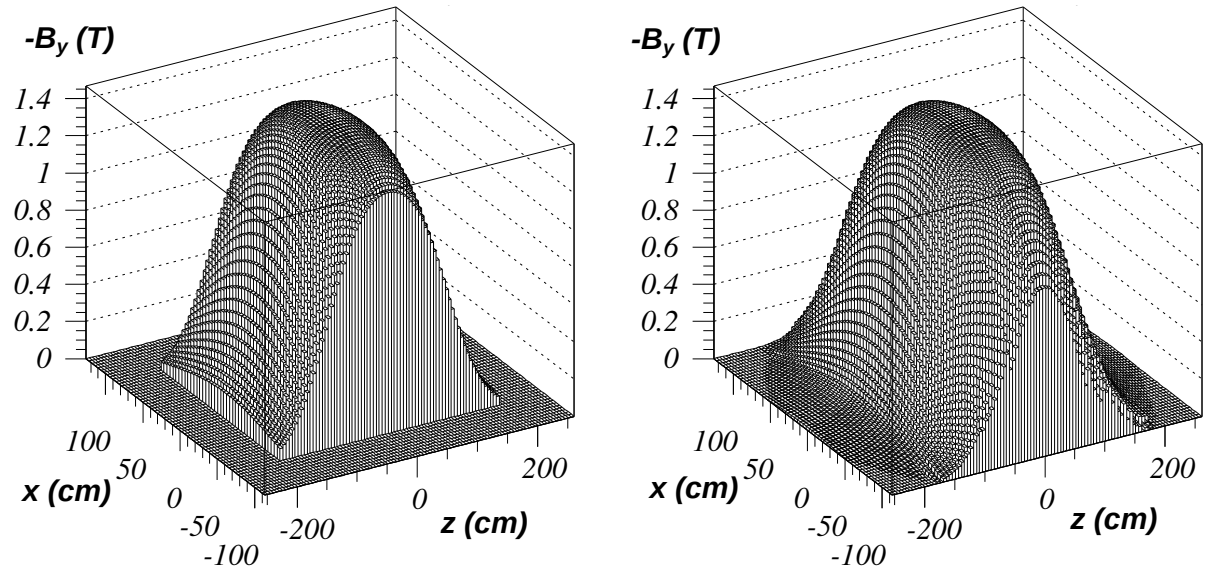

(a)

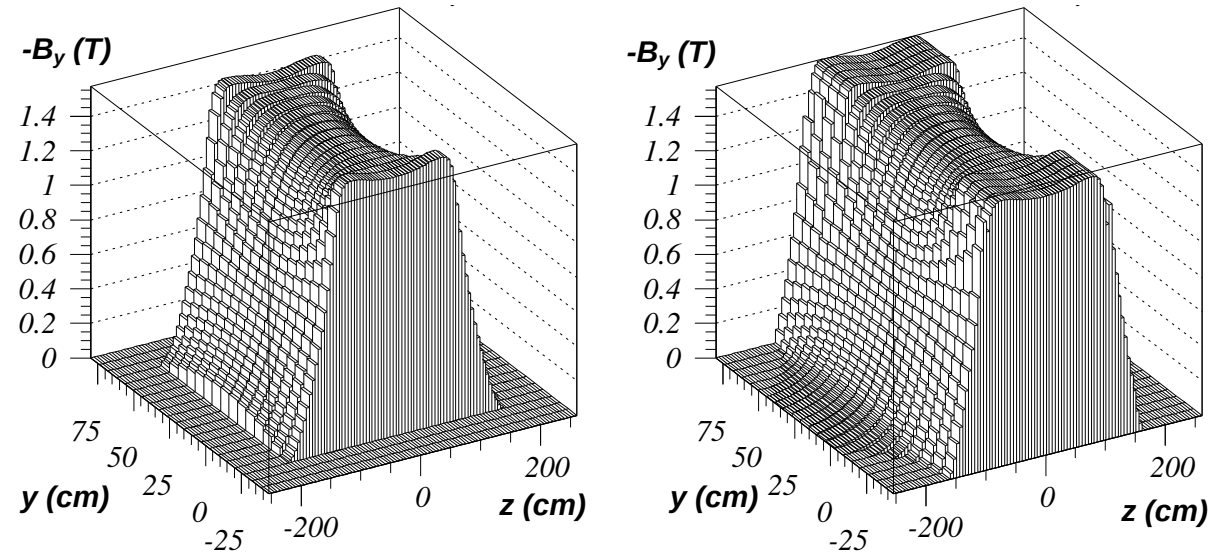

(b)

Figure 2: Goliath field maps. Top (a) shows B_y as a function of (z, x) at y = 0. Bottom (b) shows B_y as a function of (z, y) at x = 0. Measured field values on the left, extended field values on the right.

power converters designated "GOLIATH" and "DAVID". GOLIATH provides a current to both coils, whereas DAVID provides an additional current to the bottom coil to ensure a homogeneous magnetic field because of the different number of windings. The three configurations with which data was taken are shown in Table 1.

Table 1: Three configurations of the Goliath magnetic field.

Field	GOLIATH current	DAVID current
Nominal	3600 A	1600 A
Intermediate	2400 A	1166 A
Zero	0 A	0 A

Table 2: Data taken with three configurations of the Goliath magnetic field.

Field	raw S01 counts	spills
Nominal	2.81×10^{11}	20128
Intermediate	2.4×10^{10}	1552
Zero	2.3×10^{10}	1445

4 Data

20128 useful (for analysis) spills were recorded amounting to 2.81×10^{11} not normalized, raw SC01 counts. Table 2 shows the amount of data taken with the three magnetic field configurations.

For a description of the DAQ framework see [6] and a description of the trigger and DAQ conditions during data taking see [7].

5 Normalization

The calculation of the number of POT delivered to the experiment must take the different signal widths and dead times of the various scintillators into account. In addition to this, some protons, the so-called halo, might fall outside the acceptance of S1 and will only be registered by S0. If there is an accidental overlap of a proton triggering S1 during this time interval, these protons can produce a muon which triggers S2 [8].

To obtain a constant number of POT/μ-event the dead time from the S1 counter has to be increased from the nominal 30 ns to an effective 50 ns (see Figure 3(b)). However, this only applies to rates below $\sim\ 3 \times 10^6$ protons/s.

The number of POT/μ-event with at least one muon reconstructed is 710 ± 15 (syst.) for events with a nominal magnetic field and 625 ± 15 (syst.) for events with an intermediate magnetic field. For a given geometric acceptance, the muon momentum distribution is the driving force behind this difference. For larger field strengths, more low momentum muons are swept out and do not reach the downstream stations. Figure 3 shows the number of μ-event/POT with at least one muon reconstructed as a function of the S1 flux for the two magnetic field configurations.

The systematic error of 15 POT/μ-event accounts for the variation between runs. The trigger inefficiency is less than 1‰ and is hence neglected.

Applying this normalization to the 20128 spills that were used for the analysis we

conclude that this data set corresponds to $(3.25 \pm 0.07) \times 10^{11}$ POT.

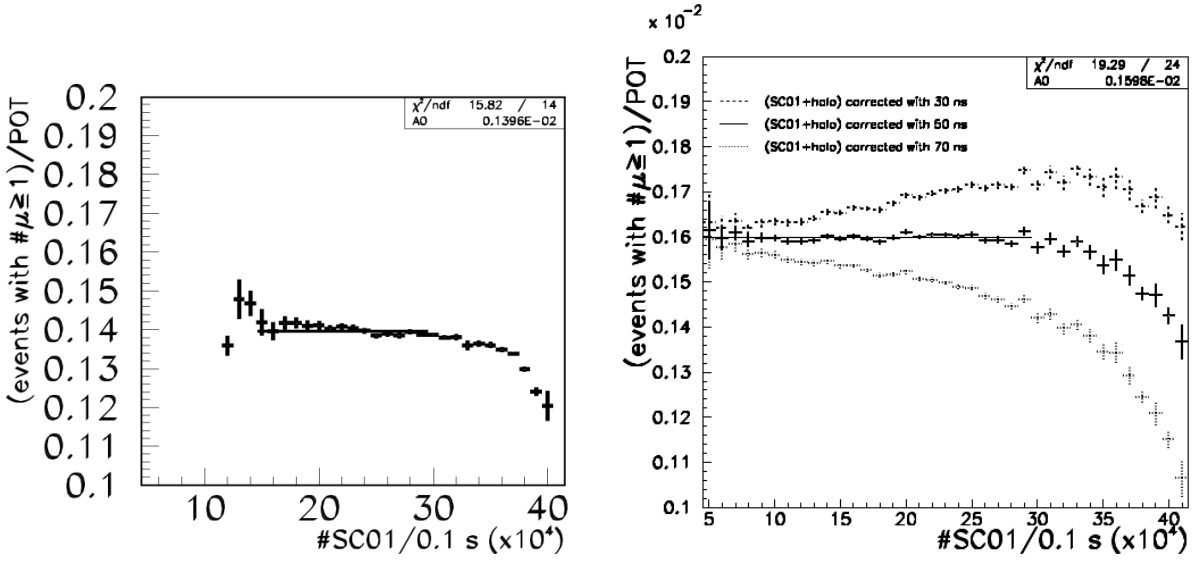

(a) (b)

Figure 3: The number of POT per event with at least one muon reconstructed as a function of the S1 flux for three assumptions on the dead time. The fit gives 710 ± 15 POT/$\mu-$event for events with the nominal magnetic field (a) and 625 ± 15 for events with the intermediate field (b).

6 Calibration

6.1 Drift tube r-t calibration

The relation between the measured drift time and the distance of the track to the wire is obtained from the TDC distribution by assuming a uniformly illuminated tube. This is done in groups of 12 channels over different layers per station following the gas flow to compensate for the drop of gas pressure. To obtain a clean TDC distribution, low occupancy events are selected (events with at least 2 and a maximum of 6 hits per tracking station). A track reconstruction only based on the channel numbers is used. Only the TDC information of hits which are < 4 cm to a reconstructed track is used. The minimum and maximum drift times are extracted from this distribution (see Figure 4 and Figure 6). These correspond respectively to tracks traversing the tube close to the wire and close to the tube wall respectively. They define the overall scale together with the minimum (0 cm) and maximum drift radius (1.815 cm). The TDC distribution is then integrated to obtain the radius to drift time relation (r-t relation, see for instance [9]), which is stored together with the data, see Figure 5. By plotting the difference between the distance of a track to the wire and the drift radius as a function of the drift radius, see Figure 7(a), it was

found out that this first order correction causes a bias in the drift radius determination. Applying a second order correction to the r-t calibration based on the empirical finding, the bias could be resolved, see Figure 7(b). The net effect of this correction is also an improvement in the hit resolution, which changed from an average of about 520μm to 370μm.

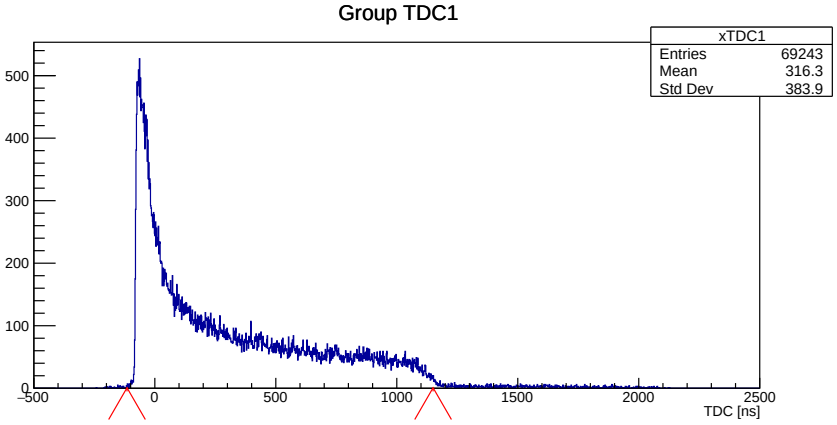

Figure 4: TDC distribution of 12 channels for low occupancy events together with estimates of T_{min} and T_{max}.

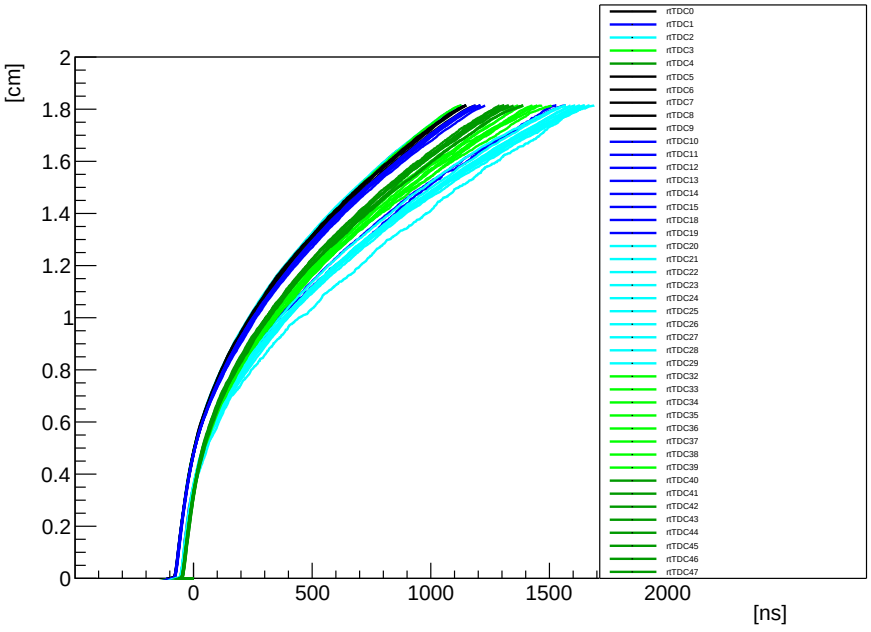

Figure 5: RT relations for all channels.

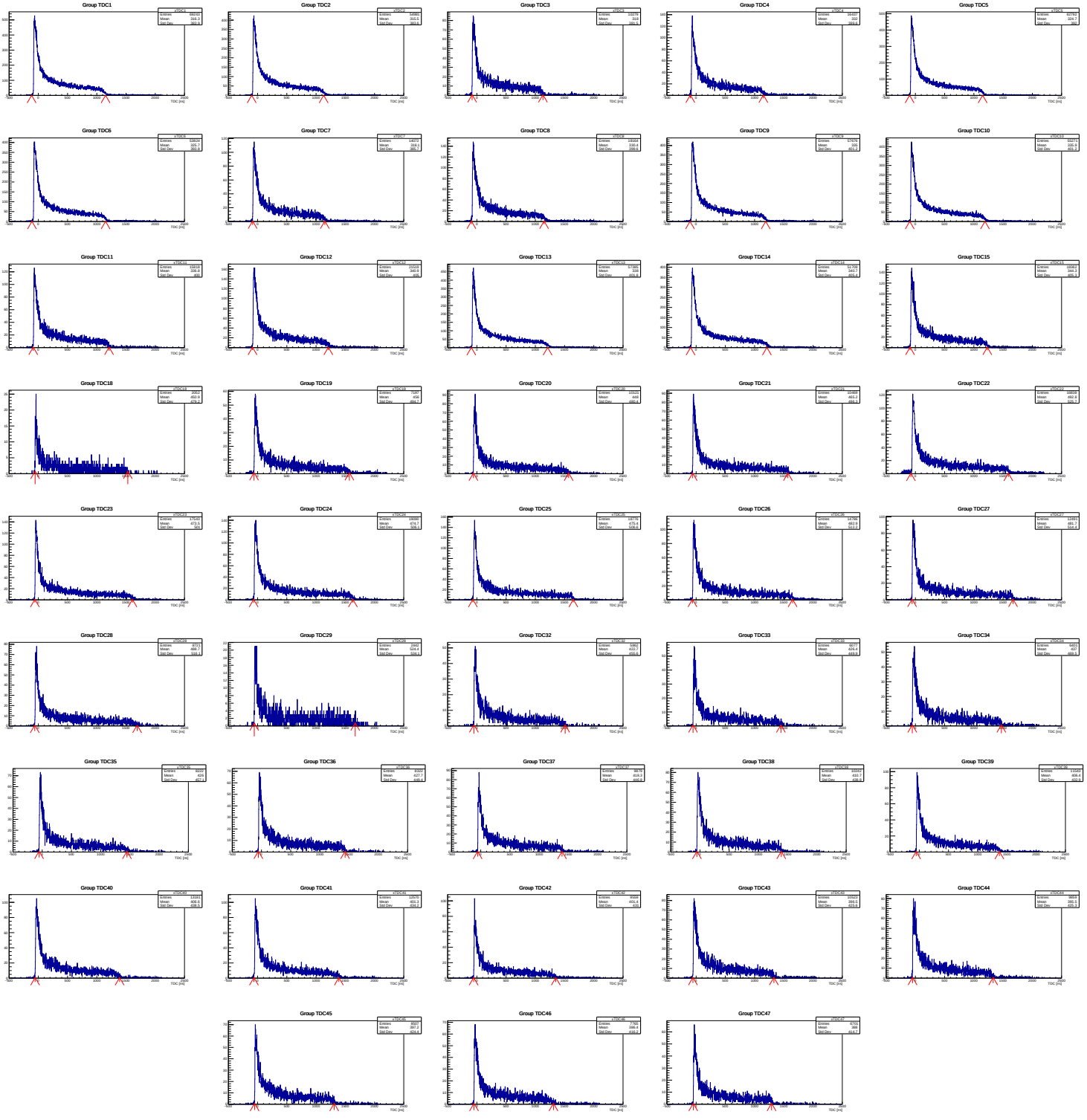

Figure 6: TDC distributions for all groups of 12 channels.

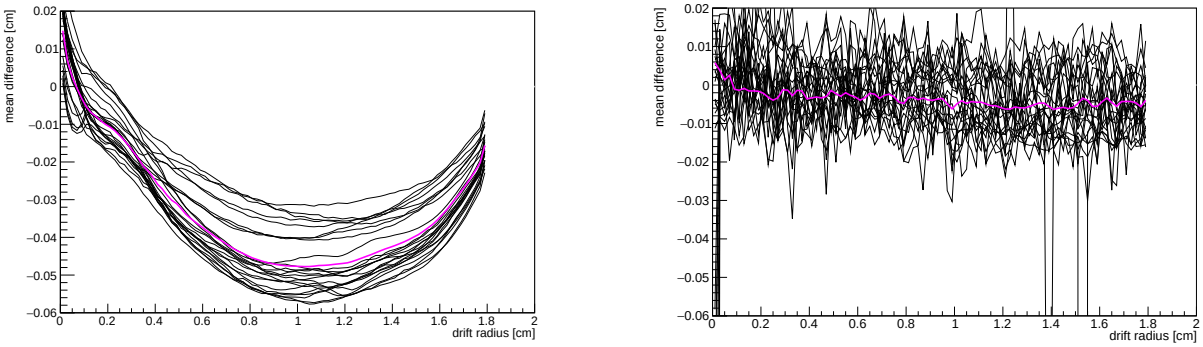

(a) (b)

Figure 7: The difference between the distance of a track to the wire and the drift radius vs drift radius, before (a) and after correction to the RT calibration (b).

6.2 Alignment and hit resolution

As a first approximation, the positions of the drift tube and RPC stations are obtained from the survey measurements (see Section 2). By looking at the biased residuals[2], the drift tube wire positions were corrected until the mean of the biased residuals were well below the nominal resolution of 270 μm, as shown in Table 3 and Figure 8. This was done with a small fraction of the data, but using the complete dataset it was confirmed that the mean residuals stay close to zero for the whole period of data taking. The expected hit resolution based on the OPERA results is 270 μm, which was set as baseline in the MC simulation. The measured average hit resolution is slightly worse, see Figure 9, and the MC has been adjusted for this, see also Table 3.

[2]i.e. closest distance of a track to a hit, with two solutions for the hit positions, drift tube centre $\pm$ drift radius.

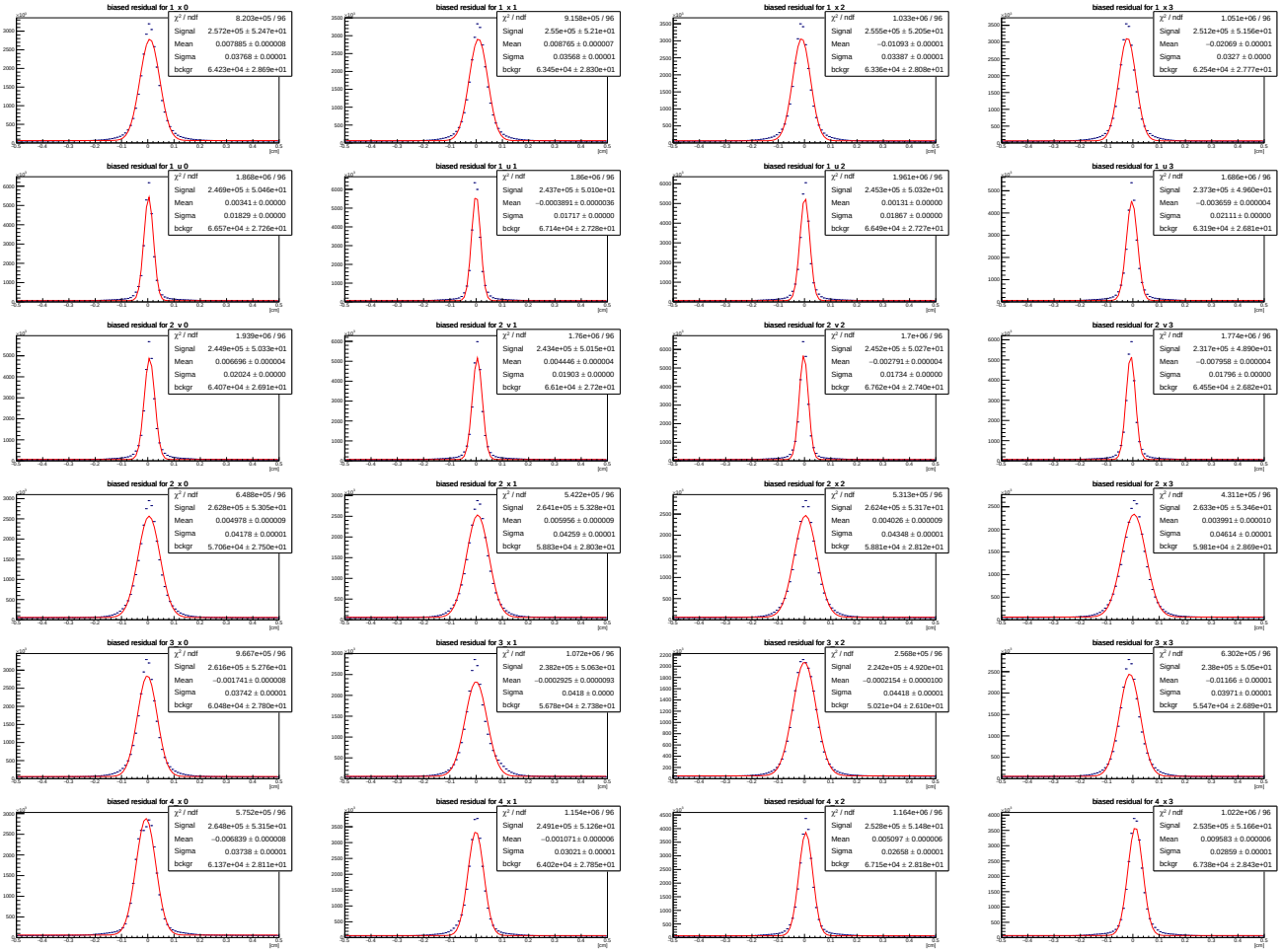

Figure 8: Biased residuals for all stations and layers. The signed distance of a track to the wire and the estimated drift radius using the RT relation and measured drift time is plotted. There are two entries per hit to account for the left/right hit ambiguity. Gaussian fits are made to obtain a mean value for the correct wire position and an estimate of the hit resolution.

Table 3: Residuals for all stations and layers.

Spill with nominal field					MC data				
station	view	layer	mean [mm]	RMS [mm]	station	view	layer	mean [mm]	RMS [mm]
1	x	0	0.08 ± 0.01	0.38 ± 0.01	1	x	0	-0.00 ± 0.00	0.36 ± 0.00
1	x	1	0.09 ± 0.01	0.36 ± 0.01	1	x	1	0.00 ± 0.00	0.36 ± 0.00
1	x	2	-0.11 ± 0.01	0.34 ± 0.01	1	x	2	0.00 ± 0.00	0.36 ± 0.00
1	x	3	-0.21 ± 0.01	033 ± 0.01	1	x	3	0.00 ± 0.00	0.36 ± 0.00
1	u	0	0.03 ± 0.01	0.18 ± 0.00	1	u	0	-0.00 ± 0.00	0.36 ± 0.00
1	u	1	0.00 ± 0.01	0.17 ± 0.01	1	u	1	-0.00 ± 0.00	0.35 ± 0.00
1	u	2	0.01 ± 0.01	0.19 ± 0.00	1	u	2	-0.00 ± 0.00	0.34 ± 0.00
1	u	3	-0.04 ± 0.01	0.21 ± 0.01	1	u	3	-0.00 ± 0.00	0.35 ± 0.00
2	x	0	0.05 ± 0.01	0.42 ± 0.01	2	x	0	0.00 ± 0.00	0.37 ± 0.00
2	x	1	0.06 ± 0.01	0.43 ± 0.01	2	x	1	0.00 ± 0.00	0.37 ± 0.00
2	x	2	0.04 ± 0.01	0.43 ± 0.01	2	x	2	-0.00 ± 0.00	0.37 ± 0.00
2	x	3	0.04 ± 0.01	0.46 ± 0.01	2	x	3	0.00 ± 0.00	0.36 ± 0.00
2	v	0	0.07 ± 0.01	0.20 ± 0.01	2	v	0	-0.00 ± 0.00	0.35 ± 0.00
2	v	1	0.04 ± 0.01	0.19 ± 0.00	2	v	1	0.00 ± 0.00	0.35 ± 0.00
2	v	2	-0.03 ± 0.01	0.17 ± 0.01	2	v	2	0.00 ± 0.00	0.34 ± 0.00
2	v	3	-0.08 ± 0.01	0.18 ± 0.01	2	v	3	-0.00 ± 0.00	0.34 ± 0.00
3	x	0	-0.02 ± 0.01	0.37 ± 0.01	3	x	0	0.00 ± 0.00	0.37 ± 0.00
3	x	1	-0.02 ± 0.01	0.42 ± 0.01	3	x	1	-0.00 ± 0.00	0.37 ± 0.00
3	x	2	0.00 ± 0.01	0.44 ± 0.01	3	x	2	0.00 ± 0.00	0.37 ± 0.00
3	x	3	-0.12 ± 0.01	0.40 ± 0.01	3	x	3	0.00 ± 0.00	0.37 ± 0.00
4	x	0	-0.07 ± 0.01	0.37 ± 0.01	4	x	0	-0.00 ± 0.00	0.36 ± 0.00
4	x	1	-0.01 ± 0.01	0.30 ± 0.01	4	x	1	-0.00 ± 0.00	0.35 ± 0.00
4	x	2	0.05 ± 0.01	0.27 ± 0.00	4	x	2	0.00 ± 0.00	0.35 ± 0.00
4	x	3	0.10 ± 0.01	0.29 ± 0.01	4	x	3	-0.00 ± 0.00	0.35 ± 0.00

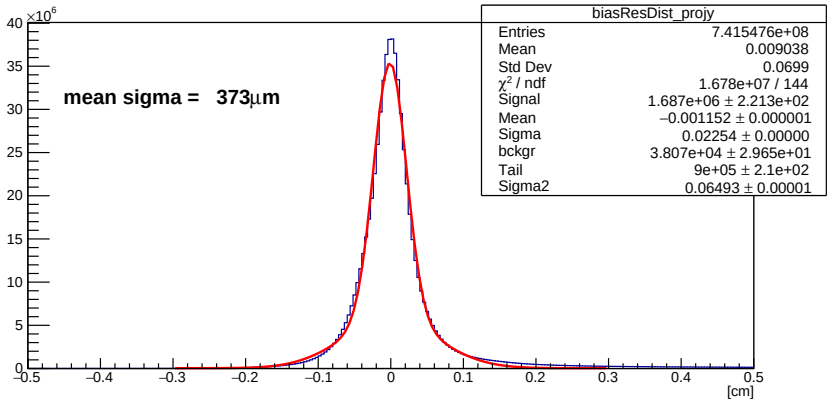

Figure 9: Average residuals of all drift tube residuals.

7 Reconstruction

The reconstruction proceeds in two steps:

1. For data, select low occupancy events (minimum 2 and maximum 6 hits per station) and make the RT relations for 3–4 spills ($>$ 350k events). This is only needed for data. In MC, the drift radius is simulated with the expected resolution.

2. Run the pattern recognition (see Section 7.1) for all events and perform a track fit (see Section 7.3) using the distance of the hits to the wire obtained from the RT relations.

The RPC tracks are reconstructed and matched to the drift tube tracks to provide muon identification.

7.1 Drift tube pattern recognition

The pattern recognition preselects hits to form track candidates and provides the starting values for the track fit. It proceeds as follows:

1. Form clusters of hits across four layers in stations 1,2 and 3,4 in the x, u and v views, requiring a minimum of 2 hits per cluster. If there are more than 2 hits per layer contributing to a cluster, these hits are discarded. The maximum cluster width is 5 cm. There should be at least one cluster in all stations and views. Large clusters of drift tube hits are split into smaller subsets, and each subset is tried.

2. Combine clusters in stations (1 and 2) and (3 and 4) to make track segments in the bending plane and fit the track segments before and after the magnet to straight lines.

3. Extrapolate the x position of the track segments to the middle of the Goliath magnet. If the difference in x between the upstream and downstream segments is smaller than 8 cm, accept the hits in the clusters to form a track candidate.

4. Add u and v clusters by checking that the y coordinate for the given x coordinate of the track segment lies in the acceptance.

5. Calculate a momentum estimate using the slopes of the track segments. Add the hits of all clusters to a list of track candidates.

7.2 RPC pattern recognition

The RPC pattern recognition proceeds similarly to that for drift tube tracks. Clusters of hits are found in the RPC stations and the clusters are combined to make tracks that are fitted to a straight line. At least hits in 3 stations are required for a track. Drift tube tracks are then extrapolated to RPC tracks. If the distance of a drift tube track to a RPC track at RPC station 1 is less than $<$ 5cm in the x-projection and less than $<$ 10cm in the y-projection, the drift tube track is tagged as a muon.

7.3 Track fitting

The coordinates of the hits forming the track candidates and the distance to the wire from the RT relations are used as input for the track fit. The track fitting is done with the GENFIT package, "a generic toolkit for track reconstruction" [10], using an iterative Kalman filter with annealing (DAF). The trackfit uses the magnetic field map (see Section 3) and the material distribution from the geometric model of the experimental setup to take into account energy loss and multiple scattering errors.

7.4 Clone removal

If tracks share more than 50% of the downstream hits, the track with the highest number of degrees of freedom is retained. This is not done for the upstream hits in order not to lose efficiency for two track events. Remaining clone tracks are rejected by taking only the track with the smallest χ^2/DoF if the cosine of the angle between two tracks is larger than 0.99995, see Figure 10.

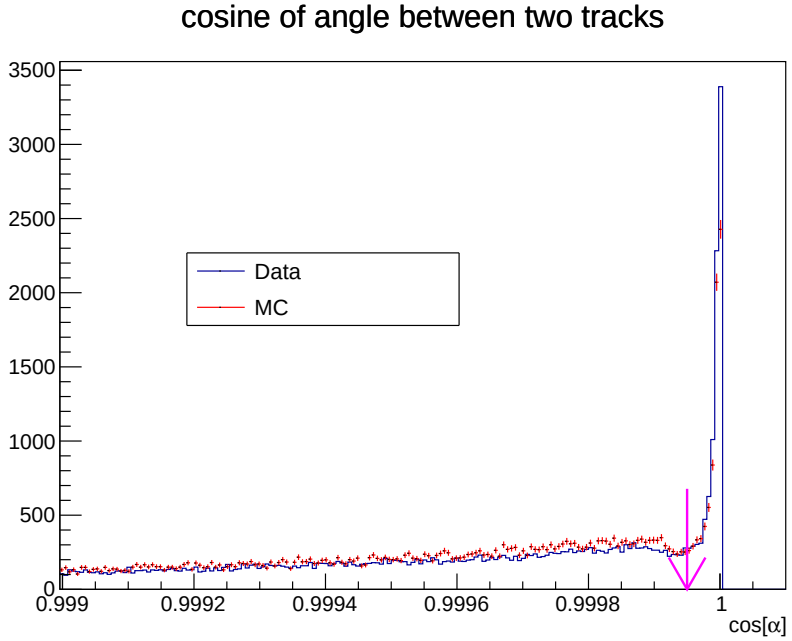

Figure 10: Cosine of the angle α between two tracks. The peak at 1 is due to very similar trajectories caused by reconstructing two tracks made with hits from the same particle. The cut used for the rejection of clones is indicated by the magenta arrow.

7.5 Momentum resolution

The momentum resolution obtained from MC is shown in Figure 11 for two values of the hit precision: 270 µm (nominal), and 350 µm (seen in data). The figure shows how the

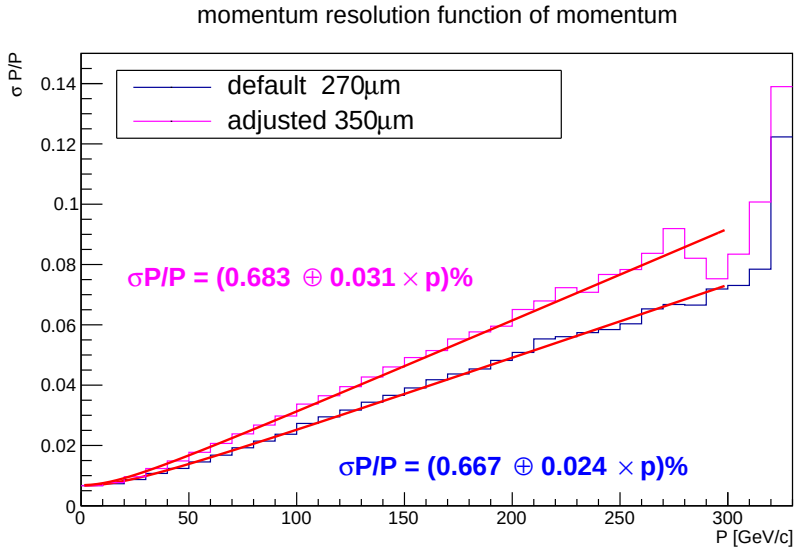

Figure 11: Momentum resolution for two values of hit precision.

less than nominal hit precision degrades the momentum resolution as a linear function of the momentum; at low momenta one can see the influence of multiple scattering.

7.6 Effect of degraded drift tube resolution

To study the impact of degraded spatial drift tube resolution the MC momentum distribution was folded with additional smearing as shown in Figure 12.

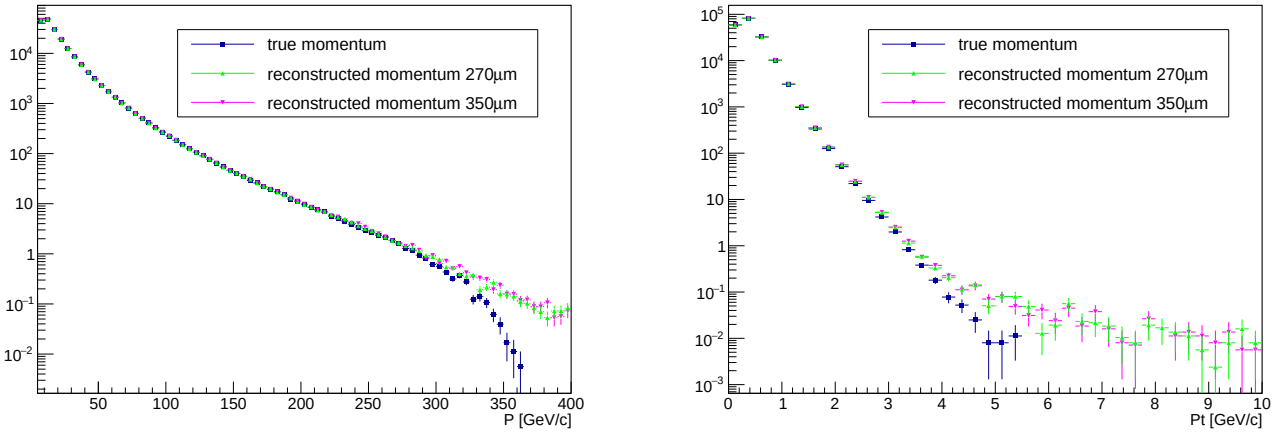

Figure 12: Effect of additional Gaussian smearing on the MC momentum distribution, left p, right p_T.

The tails towards large momentum p and p_T are caused mainly by tracks fitted with wrong drift times due to background hits.

From this we conclude that the effect of the degraded resolution of the drift tubes that we observed is negligible for our studies of the momentum spectrum.

8 Ghost tracks

Ghost tracks are badly reconstructed trajectories made from combinations of hits caused by different particles, from a second muon or from electrons and positrons, or large multiple scattering together with the limited granularity of the tracking detectors. In data, possible additional sources are noise hits from cross talk and residual misalignment. Their estimated momentum is far from the momentum of the original muon in the event. These tails dominate the momentum distribution above 350 GeV/c, see Figure 13. In MC, a ghost track can be classified as a trajectory with less than 2/3 of the measurements originating from the same MC particle. The true momentum of a trajectory is taken from the momentum of the MC particle with most measurements contributing. Figure 13 shows the momentum distribution of all reconstructed tracks (blue), together with the momentum distribution of ghost tracks (red) and perfectly reconstructed tracks, where all measurements are from the same MC particles (green), and for comparison the true momentum of a track (magenta). Although ghost tracks account for less than 1 ‰ of all tracks, they start to dominate the momentum distribution above 350 GeV/c. It can happen that a track reconstructed with all measurements from the same MC particle yields a momentum far from the original true momentum, probably due to large multiple scattering.

Ghost tracks can be reduced by requiring matching to RPC tracks. This is done for trajectories with reconstructed momentum above 10 GeV/c. Below 10 GeV/c, the muon does not have enough energy to pass through 3 RPC stations with high efficiency. However, in this momentum range, the fraction of ghost tracks is much less than 1%.

According to MC, the rate of ghost tracks above 300 GeV/c is about constant. Above 450 GeV/c, the rate of tracks is dominated by ghost tracks. This can be used to estimate the fraction of ghost tracks in data. The ratio between the number of tracks between 450 GeV/c and 500 GeV/c and the number of all tracks above 450 GeV/c is 33% in data and 39% in MC. However, in absolute terms, the number of ghost tracks (tracks between 450 GeV/c and 500 GeV/c) in data is about 3.0 times larger than in MC. This can be understood due to larger occupancies in data compared to MC which increase the probability of using wrong hits. Extrapolating the number of ghost tracks to the full momentum range yields a ratio of ghost tracks to all tracks of 0.03×10^{-3} in MC and 0.07×10^{-3} in Data.

For the final results, only trajectories below 300 GeV/c are being taking into account, in which the rate of ghost tracks should be $< 10\%$ in all momentum bins.

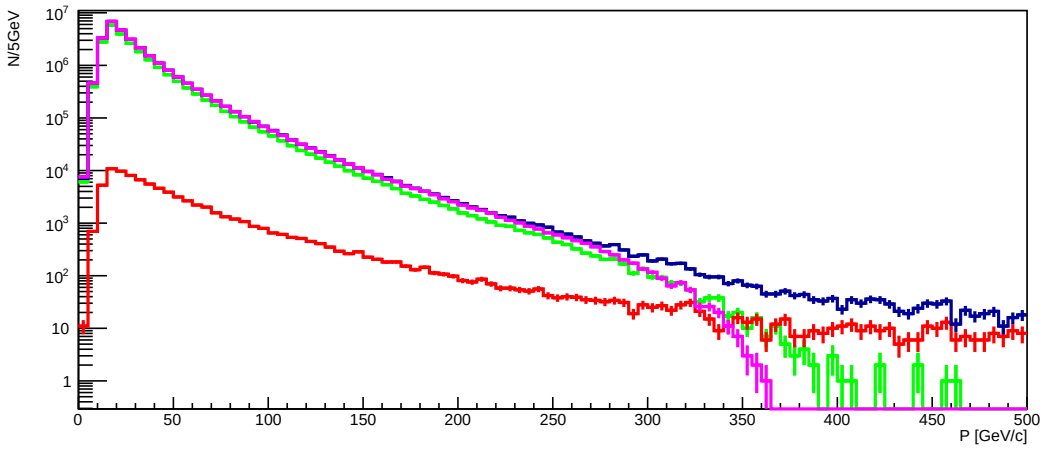

Figure 13: MC momentum distribution of all reconstructed tracks (blue), ghost tracks (red), tracks with all measurements from same MC particles (green) and true momentum distribution (magenta).

9 Data quality monitoring

Figure 14 shows the mean reconstructed momentum as a function of the run number as well as the relative number of tracks and number of muons relative to the number of tracks. The data quality is constant during the entire running period, with the exception of the early spills where the detector was being tuned and runs 2382–2396 which were taken with the intermediate Goliath field. The dip in the relative number of tracks after run 2250 is because the discriminator setting of the third drift tube PM (which was not working until then) was lowered, which increased the amount of noisy triggers.

10 Reconstruction efficiencies

Since we are not interested in absolute efficiencies, we only need to control the differences of efficiencies between data and MC. This section will discuss drift tube efficiencies estimated in data and MC with two different methods. The first using data and MC with nominal field and fitted tracks. The second method uses data with zero field, in which case a track can be reconstructed in the RPC and used to look for corresponding hits in the drift tubes. It also allows to give a direct estimate of the track reconstruction efficiency for the drift tubes. The RPC detector efficiencies can be determined by extrapolating drift tube tracks with large momentum to the RPC stations.

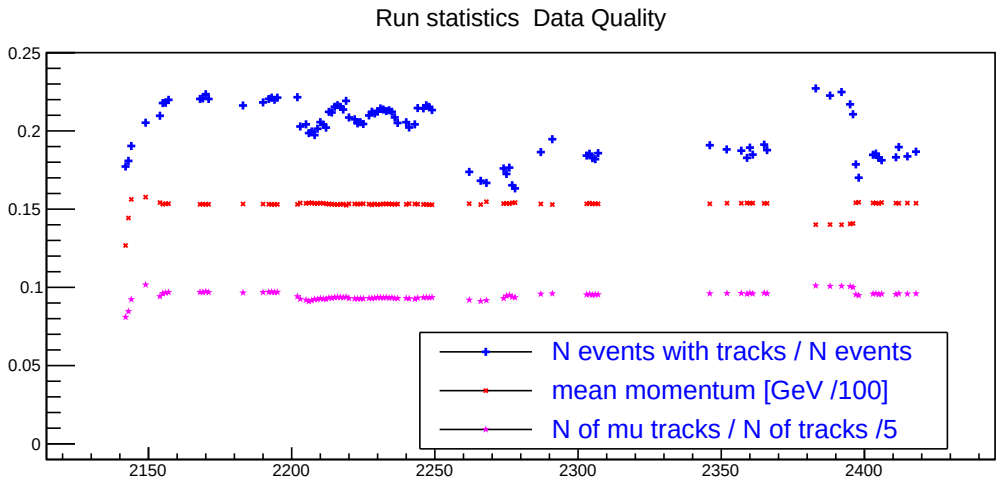

Figure 14: Data quality as a function of the run number.

10.1 Drift tube hit efficiencies using fitted tracks

Each drift tube station consists of four layers. A minimum of two hits in each station is required to make a track candidate. Due to empty space between tubes [4], the geometrical acceptance of a single layer is reduced. It is given by the inner tube diameter divided by the pitch which is 86% for vertical tracks and increases for inclined tracks (see also [3]).

Due to the fact that there is a limited number of layers, the standard method of determining the inefficiency by removing layers can not be applied. To calculate the layer hit efficiency with fitted tracks, the number of hits correlated to the track in each layer is determined. The effective efficiency per layer is then given by the ratio of correlated hits divided by the number of tracks. The tracks are confirmed with hits in the RPC station to remove badly reconstructed tracks.

In a first approach, the correlated hits are simply determined by looking at all tubes the reconstructed track has passed in a layer, counting only hits in these tubes. Since this can either be a hit or no hit, this method is called binary. The obtained efficiency using this method is 85%.

This method neither takes into account if the drift distance corresponds to the track distance nor does it account for possible random hits. Therefore a second approach is made looking at the residuals:

The track trajectory is interpolated to the z-position of a layer under study and the distance of each hit to the track in this layer is determined. Since the hit is defined only by the drift distance obtained from the rt-relation, no directional information is known and two solutions exist (left-right ambiguity). Both are filled into the histogram and fitted by a Gaussian plus background. The obtained biased residuals of all layers are shown in Figure 15. Three contributions can be seen:

1. The central peak corresponds to distances given by the true solution of the track

distance to a correlated hit.

2. The wide shoulder comes from the corresponding second solution, where the hit is close to the track, however the distance was calculated w.r.t. the opposite side of the drift-circle, thus ranging from 0 to ± the tube diameter.

3. The remaining entries are due to random hits and their number is determined in the region outside the shoulder from −6 cm to −4 cm and 4 cm to 6 cm.

By subtracting the background of random hits and taking into account that each hit is filled twice, layer efficiencies are obtained close to the geometrical limit, except for station 3, layer 1, 2 and 3 which suffer from several dead channels.

By only counting hits in the narrow peak after subtracting the background from the shoulder between −3.5 cm and 3.5 cm, about 4%–5% lower efficiencies are obtained (see Figure 16). This is mainly due to a uncorrelated drift time caused by another particle firing the same drift tube (e.g. delta electrons, see Section 10.4).

The efficiencies obtained from the MC simulation[3] are 86%. The efficiencies for station 3 layer 1, 2 and 3 are slightly lower (see Figure 16).

The difference between data and MC could be due to the presence of more delta rays in data than in MC. However, delta rays are mainly seen in upstream stations, while the difference between data and MC is the same for all layers. In addition, delta rays are present in MC, but do not seem to have a big impact on the layer efficiency there.

This method gives a first estimate of the MC to data agreement, but cannot directly be used to obtain tracking efficiencies.

[3]Dead channels were incorporated in the MC.

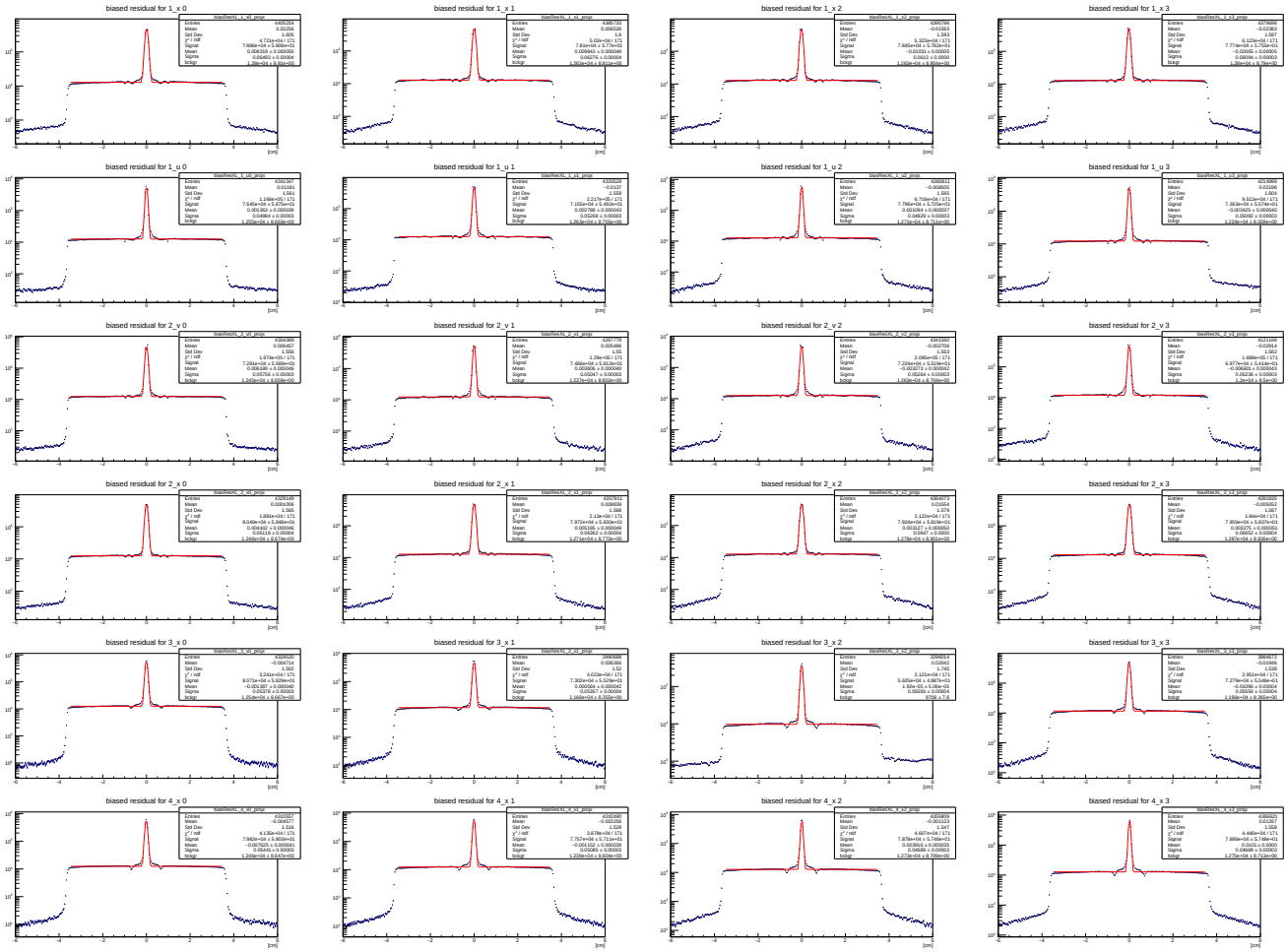

Figure 15: Distribution of biased residuals to determine hits correlated to fitted tracks. The fit is only used to determine the flat background outside of the peak, from ±1cm to ±3.5cm

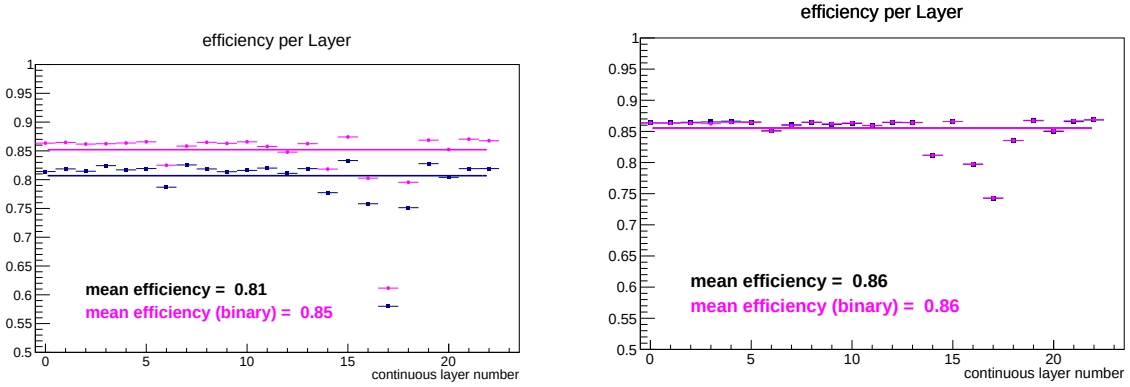

Figure 16: Drift tube layer hit efficiency estimated from biased residuals in data (left) and Monte Carlo (right) as function of the layer number starting with zero for first layer in station 1 up to 23 for last layer in station 4.

As a cross-check the efficiencies were also computed in a slightly different way. For a reconstructed track the correlation of a hit is determined purely by the fit. For each hit, the fit determines a weight between 0 and 1, 0 meaning that the hit is rejected. The weight is shared among both possible options resulting from the left-right ambiguity, ideally rejecting the wrong side and giving a high weight to the true side. Taking the sum of the weights gives a measure of the correlation of a hit to the track. Hence, summing up all weights of the hit in a layer gives the number of correlated tracks. Again, the number of correlated hits in each layer was then divided by the number of tracks giving the efficiency. The results are shown in Figure 17, compared to the previous method they are slightly higher yet comparable.

10.2 Drift tube hit efficiencies using RPC tracks

With zero field data, it is possible to extrapolate track segments found in the RPC stations to any of the drift tube station by using a linear track extrapolation (see Figure 18). Once a track is confirmed by matching it to hits in a drift tube station, the track parameters can be refined using the hit positions of this tagging station. The best precision is obtained with the station furthest away from the RPC stations, drift tube station 1 or 2. Using Figure 19, which shows the distance of the hits in any of the other drift tube stations, one can extract the number of correlated hits by subtracting the background estimated from the sidebands from the total number of hits.

This gives an independent estimate for the drift tube layer efficiency (see Figure 20). It is comparable to the biased efficiencies obtained with full field and binary resolution in Section 10.1.

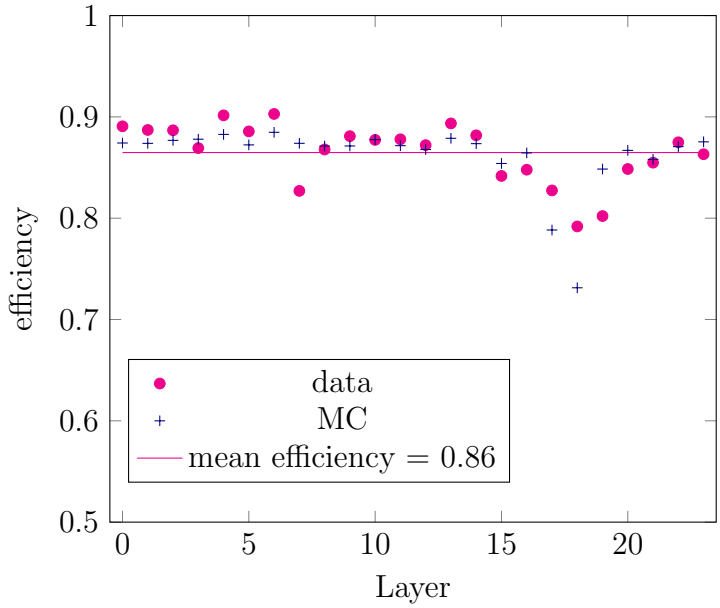

Figure 17: Drift tube layer hit efficiency estimated purely from fit results

10.3 Tracking efficiency in data

The inefficiency per drift tube station is relevant for the track reconstruction efficiency. It can be determined by looking at events with less than 2 hits in a given station close to a tagging track, see Figure 21. The inefficiencies are 0.05%, 0.02% 0.17% 0.09% for the drift tube x-stations $1-4$. Assuming the stereo layers have similar inefficiencies the resulting inefficiency for 6 stations is $\sim 0.5\%$.

To determine the tracking efficiency, we use the RPCs to identify muon tracks in data with the magnetic field switched off. These straight muon tracks are extrapolated to drift tube station T1x, and the hits in all 4 layers within a given search window are counted. If more than 2 hits are found, the track is counted as a"true track". We then count how often the the fitting procedure is successful and find:

$$\begin{aligned} \epsilon_{data}\ (\text{drift tube tracking}) &= \frac{N_{\text{fitted tracks}}}{N_{\text{true tracks}}} &&= 96.1\% \\ \epsilon_{data}\ (\text{muon tracking}) &= \frac{N_{\text{fitted tracks tagged as muon}}}{N_{\text{true tracks}}} &&= 93.6\% \end{aligned} \tag{1}$$

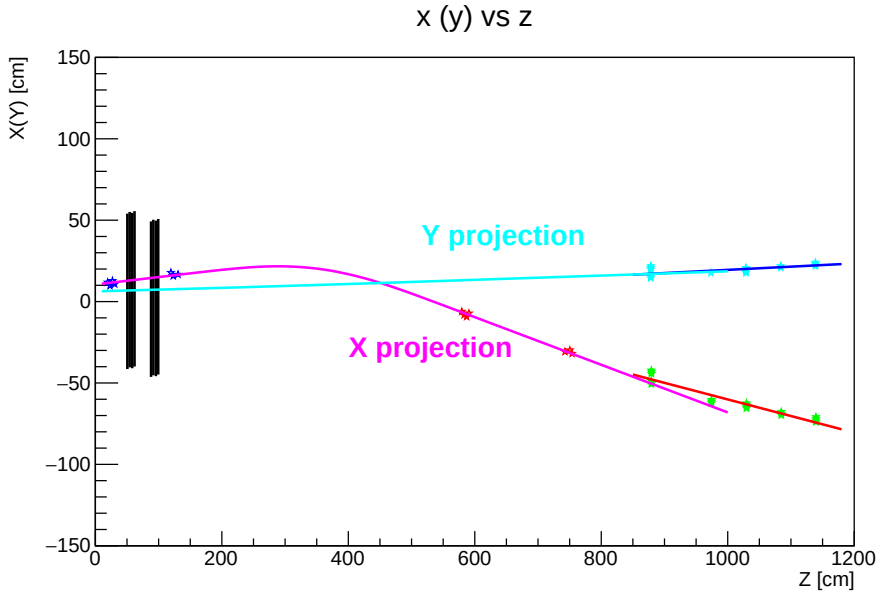

Figure 18: Display of an event with reconstructed DT and RPC tracks in X- and Y-Z projection.

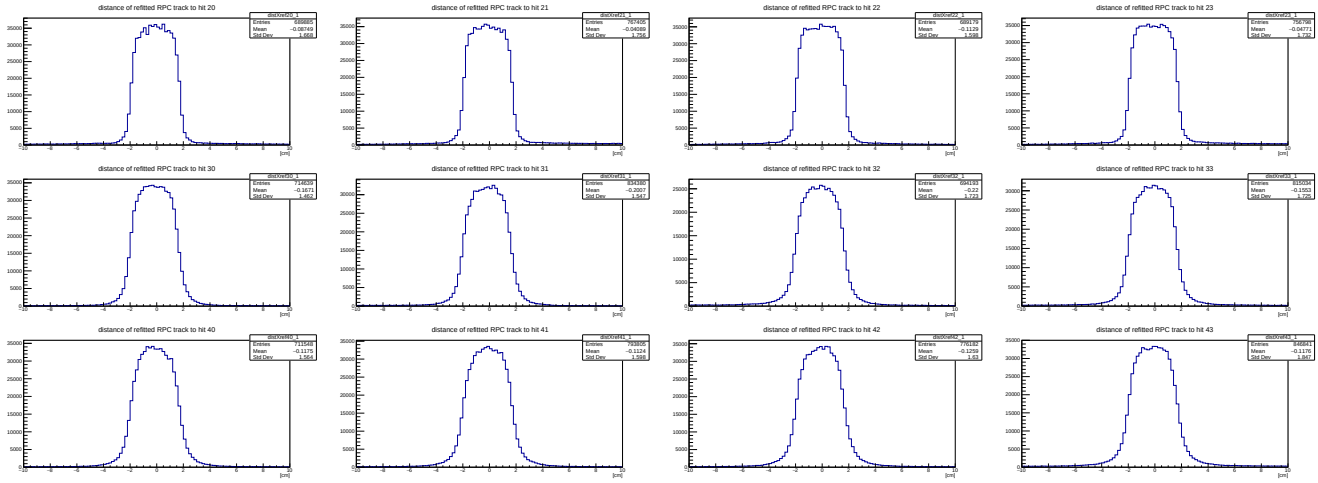

Figure 19: Distances of any hit in the four layers of the DT stations 2, 3 and 4 to a straight line defined by the RPC track position in RPC station 1 and hits in DT station 1. The hits correlated with the extrapolated track are obtained by subtracting the background estimated from the sidebands from the total number of hits.

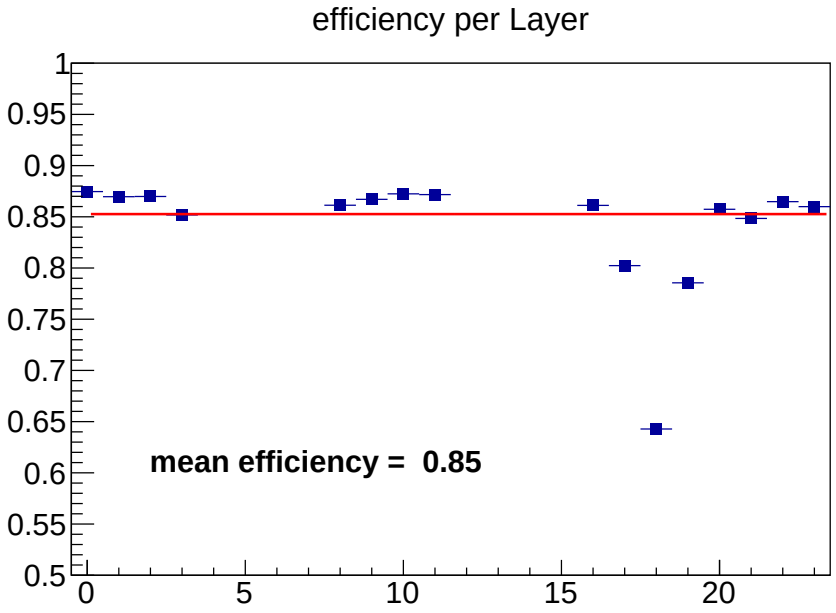

Figure 20: DT Layer efficiencies, starting with zero for first layer in station 1 up to 23 for last layer in station 4. The u and v layers are skipped.

10.4 Tracking efficiency in MC

A "reconstructible drift tube track" is defined as a track that crosses all 6 drift tube stations (4 plus 2 stereo views). Then:

$$\epsilon_{MC}\ (\text{drift tube tracking}) = \frac{N_{\text{fitted drift tube tracks}}}{N_{\text{reconstructible drift tube tracks}}}$$

A"reconstructible drift tube and RPC track" is a reconstructible drift tube track that crosses more than 2 RPC stations. Then,

$$\begin{aligned}\epsilon_{MC}\ (\text{muon tracking}) &= \frac{N_{\text{fitted drift tube tracks tagged as muons}}}{N_{\text{reconstructible drift tube and RPC tracks}}} \\ &= 96.6\%\ (\text{MC with nominal magnetic field})\end{aligned}$$

By visually studying the events for which the track reconstruction failed, it was seen that these events suffer from additional hits. The additional hits are caused by electrons and positrons produced in electromagnetic processes in the last radiation length of the hadron absorber (delta rays). They cause additional hits which confuse the pattern recognition. More severe is the case in which they hit the same drift tube as the muon. For a given hit, only the shortest drift time is used in the reconstruction. With an additional particle traversing the same drift tube, it is likely that a wrong drift time is used, which leads to either failure of the track fit or wrong estimates of the track parameters. The track efficiency is therefore studied as function of the upstream station occupancy (see Figure 22 and Figure 23).

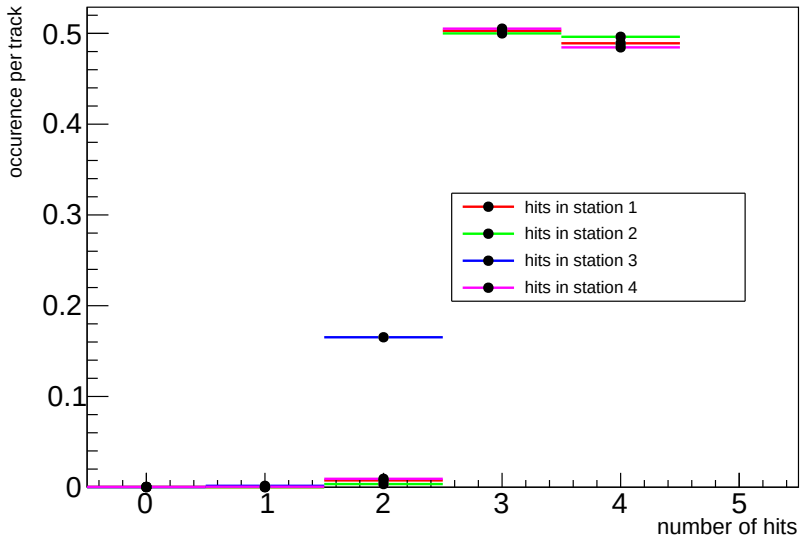

Figure 21: Number of hits associated to tracks in station 1, 2, 3 and 4 respectively (data). The events with 0 or 1 hit in any of these stations lead to a tracking inefficiency.

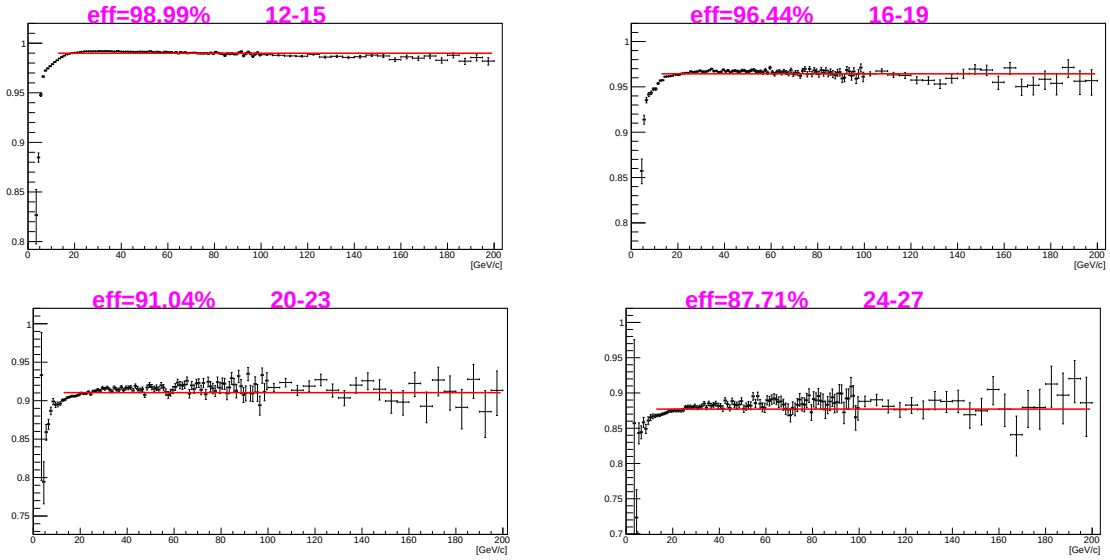

Figure 22: Tracking efficiency in MC as function of true momentum for different upstream station hit occupancy, $12-15$ hits, $16-19$, $20-23$ and $24-27$.

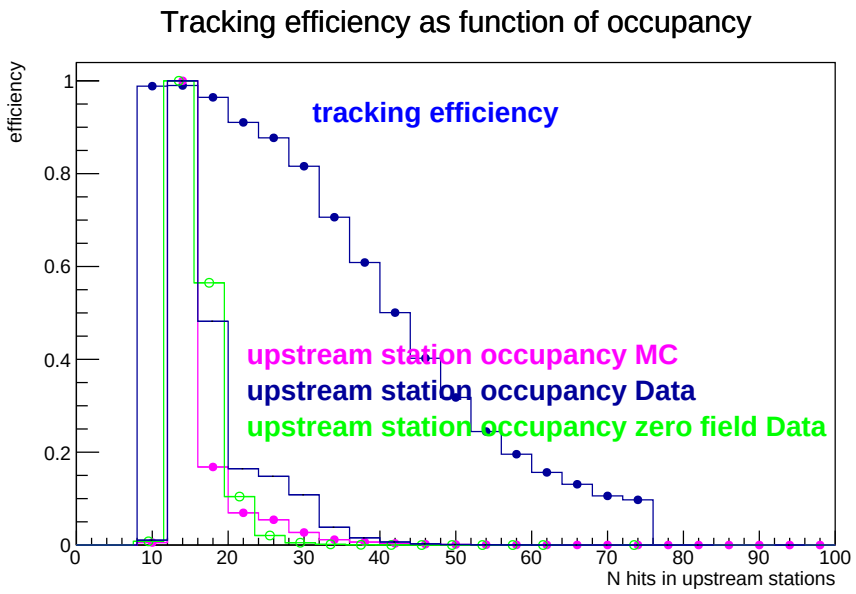

Figure 23: Tracking efficiency in MC as function of upstream station hit occupancy (blue), together with the distribution of upstream station occupancy in MC (magenta) and Data (nominal field blue and zero field green).

The average tracking efficiency in MC is 96.6% including matching to RPC tracks for reconstructible trajectories. Weighting the MC tracking efficiencies with the upstream station occupancy observed in data, an average efficiency of 94.8% is obtained. Hence the MC yields need to be corrected by −1.8%.

With the upstream station occupancy observed in zero field data, an average trackinge efficiency of 96.9% is predicted:

ϵ_{MC} (muon tracking with field off data occupancies) = 96.9%

We take the difference between the predicted MC estimate (96.9%) and the measured estimate (93.6%, see Section 10.2) as a systematic error: 3.3%.

10.4.1 Delta rays

It is not expected that the number of delta rays is different in data with zero field compared to data with nominal field. However, it could happen that the delta rays in zero field data do not show up as additional hits, but stay closer with the muon track and are only a source of wrong drift time. This could explain why the MC estimate using the zero field data occupancy gives a much larger efficiency than measured.

In general, the upstream station occupancy is qualitatively well reproduced in the simulation, Figure 24). A future detailed study could quantify the difference between data and MC, which would give important information about the validity of the electromagnetic background in the SHiP simulation of the active muon shield.

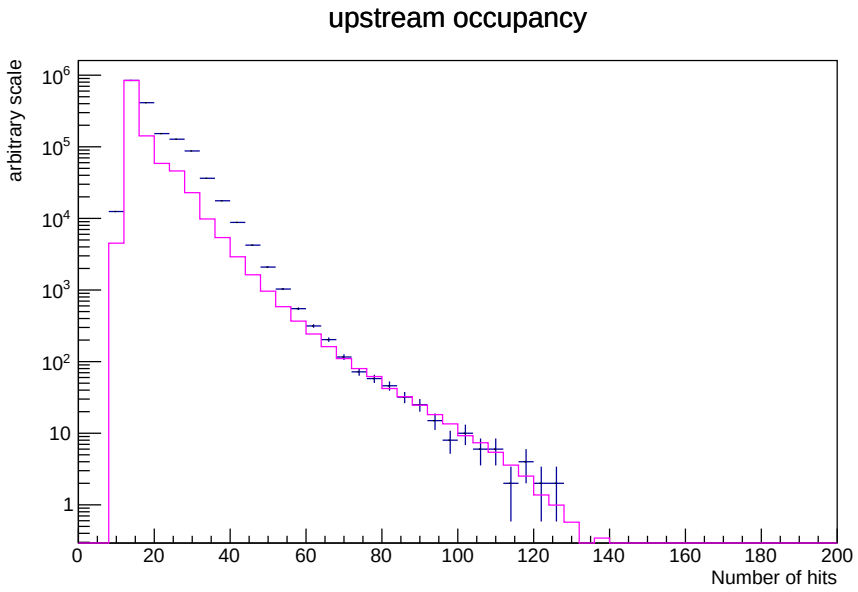

Figure 24: Upstream station occupancy in MC (magenta) and Data (blue) for events with a reconstructed track.

10.5 RPC detector efficiency

Efficiencies are determined by extrapolating a drift tube track to the RPC stations (see Figure 25). If an RPC hit in station $s+1$ view x(y) is matched to a track (within a window of 10 cm), we count how often a hit in station s view x(y) is also matched. This is done as a function of track momentum. Single hit efficiencies above 10 GeV/c are typically around 98%, (see Figure 26). The efficiency in station 3 drops as function of momentum due to the location of three dead channels (see Figure 27) around $X \sim 0$. For low momenta, most of the tracks pass on the left or right of the dead channels (see Figure 28(a)) and no inefficiency is observed. For higher momenta, the tracks are more centered at $X = 0$ (see Figure 28(b)), where the dead channels contribute to the inefficiency.

For a muon track, hits are required in three out of five stations, which leads to a muon identification efficiency close to 100%. Thus no correction to the MC is required.

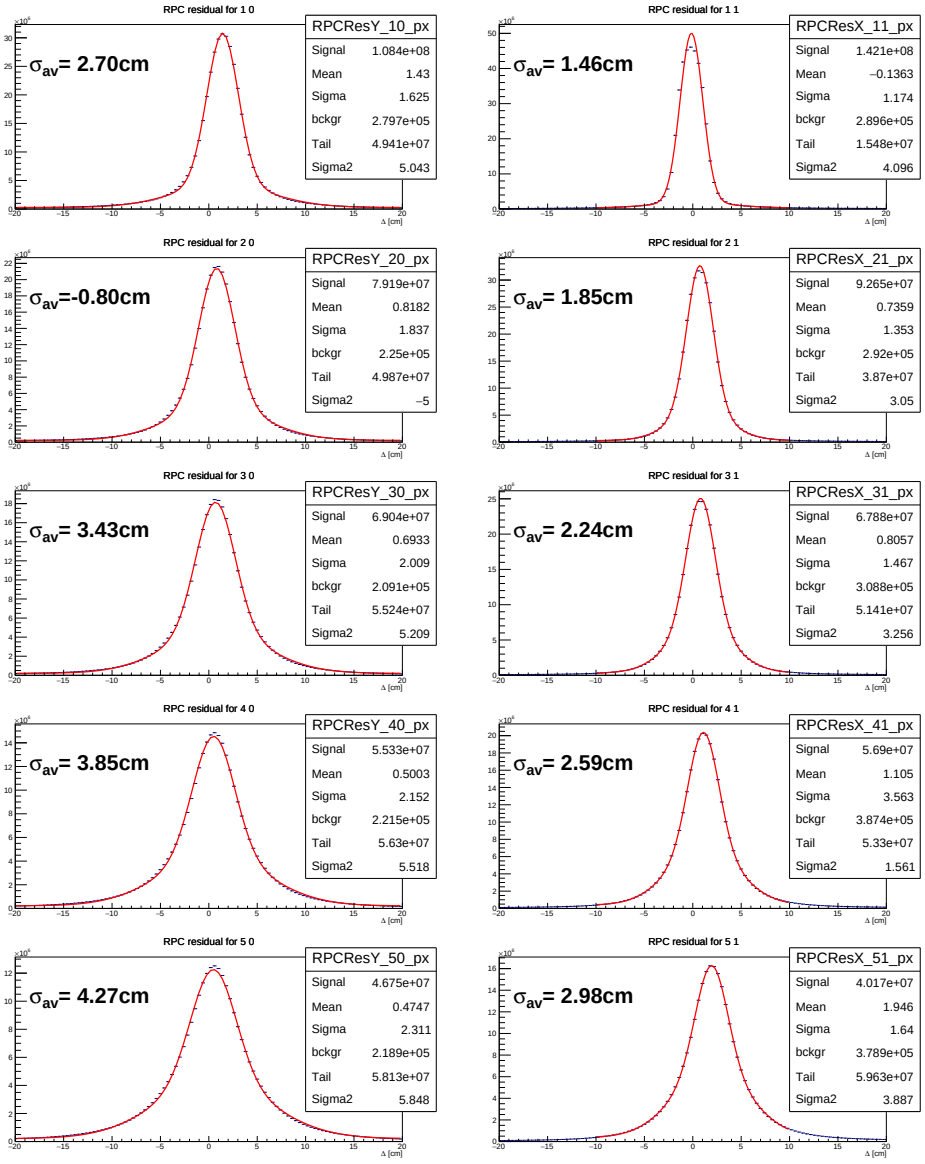

Figure 25: RPC residuals, distance between the track extrapolation and a hit in the RPC stations 1 to 5 (top to bottom) for X (right) and Y (left) projection.

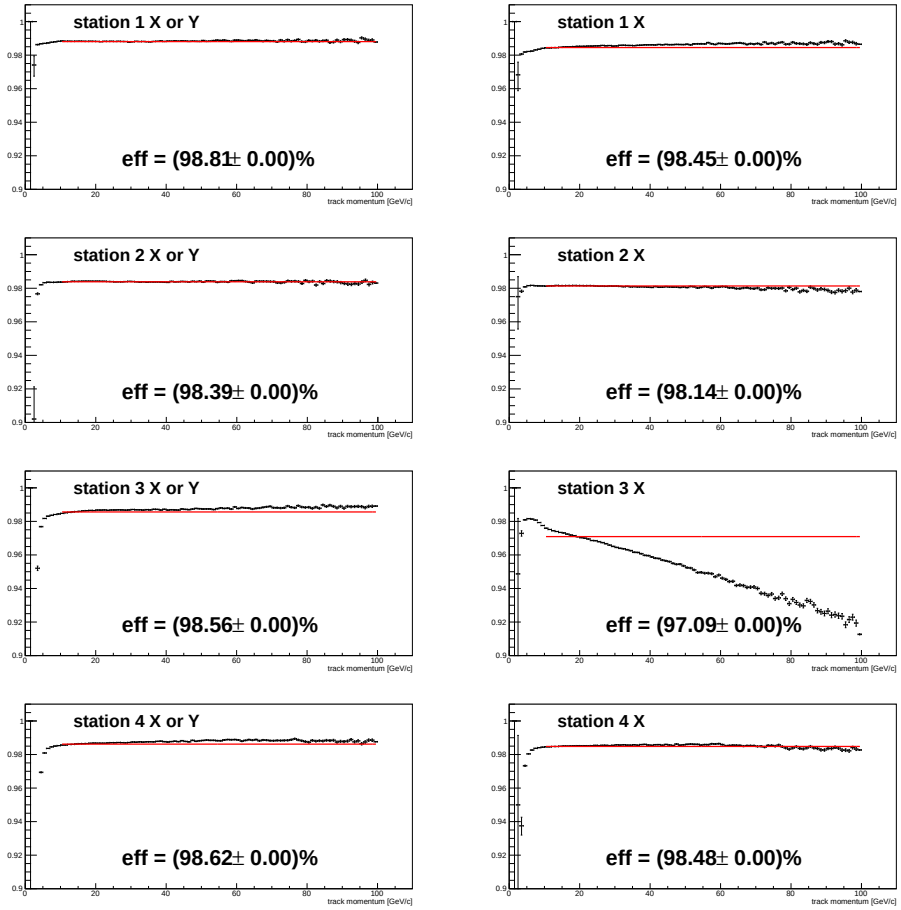

Figure 26: RPC hit efficiency per station. The efficiency drops as function of momentum for station 3 X is due to 3 dead channels centered around $X = 0$ (see text and Figures 27, 28(a) and 28(b)).

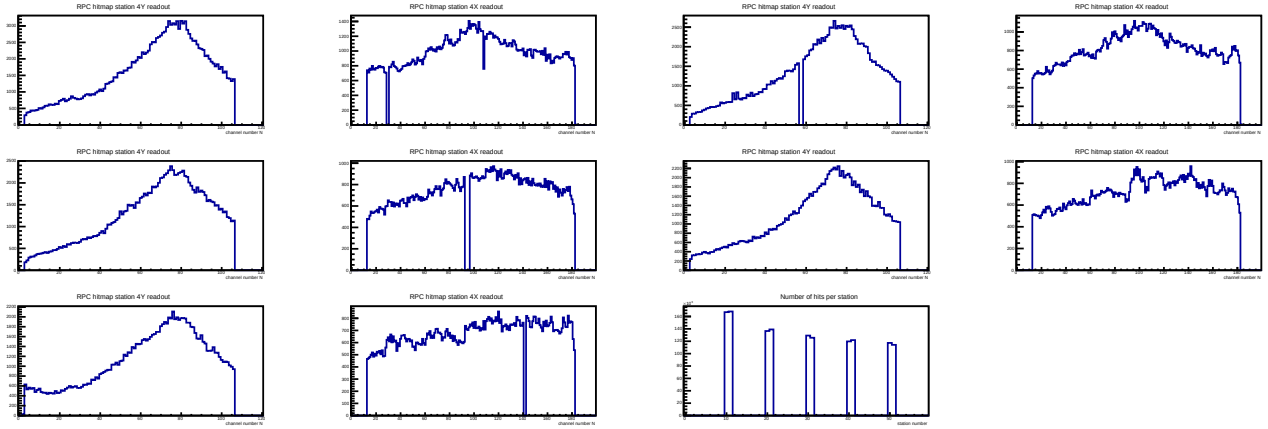

Figure 27: Hitmaps of the 5 RPC stations, X and Y readout, indicating the location of dead channels. The last figure shows the sum of hits in the 5 stations.

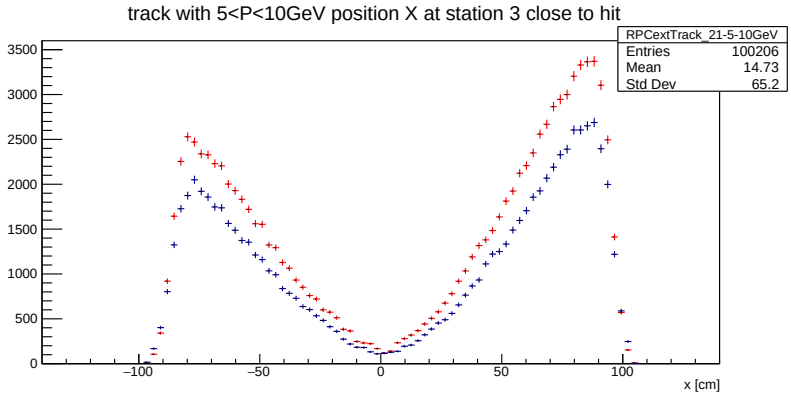

(a)

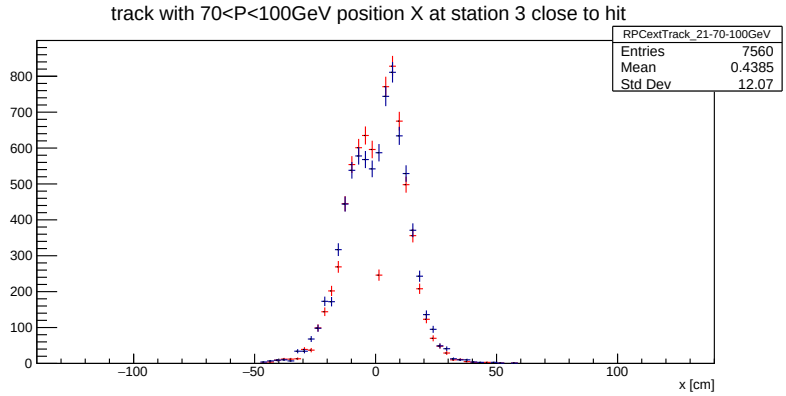

(b)

Figure 28: X-position of tracks in station 3 (red) and station 4 (black, for comparison) with hits matched to tracks. a) Low momentum tracks, b) High momentum tracks.

11 Comparison with Monte Carlo data

A large sample of muons was generated (with Pythia6, Pythia8 [11] and Geant4 [12] in FairShip) for the background studies of SHiP, corresponding to the number of POT as shown in Table 4. The energy cuts of 1 GeV and 10 GeV were imposed to save computing time. The primary proton nucleon interactions are simulated by Pythia8, with the settings:

```
"SoftQCD:inelastic = on";
"PhotonCollision:gmgm2mumu = on";
"PromptPhoton:all = on";
"WeakBosonExchange:all = on";
```

The emerging particles are transported by GEANT4 through the target and hadron absorber producing a dataset of so called mbias events. A special setting of GEANT4 was used to switch on muon interactions to produce rare dimuon decays of low mass resonances:

```
geant4 physics list: "QGSP_BERT_HP_PEN"
geant4 setting for muons:
/physics_lists/em/PositronToMuons true
/physics_lists/em/GammaToMuons true
```

Since GEANT4 does not have production of heavy flavor in particle interactions, an extra procedure was invented to simulate heavy flavor production not only in the primary pN collision but also in collisions of secondary particles with the target nucleons. For performance reasons this is done with Pythia6. The mbias and charm/beauty datasets were combined by removing the heavy flavour from the mbias and inserting the cascade data with appropriate weights. See [13] for the details of how the full heavy flavour production for both the primary and cascade interactions was obtained.

Table 4: MC samples made for SHiP background studies.

$E_{kin} > E_{min}$	mbias/cascade	POT
1 GeV	mbias	1.8×10^9
1 GeV	charm ($\chi_{c\bar{c}} = 1.7 \times 10^{-3}$)	10.2×10^9
10 GeV	mbias	65.0×10^9
10 GeV	charm ($\chi_{c\bar{c}} = 1.7 \times 10^{-3}$)	153.3×10^9
10 GeV	beauty ($\chi_{b\bar{b}} = 1.3 \times 10^{-7}$)	5336.0×10^9

The data prepared for SHiP assumes a 5 m hadron absorber, while the hadron absorber used in this experiment was only 2.4 m long. Figure 29 shows the incoming versus outgoing muon momentum obtained from the Geant4 particle gun on 2.5 m iron. This figure shows that all muons going into 2.5 m iron with a momentum > 5 GeV/c survive the extra 2.5 m iron with a momentum > 1 GeV/c. Thus the data can be compared to the MC for $p > 5$ GeV/c (ignoring resolution effects).

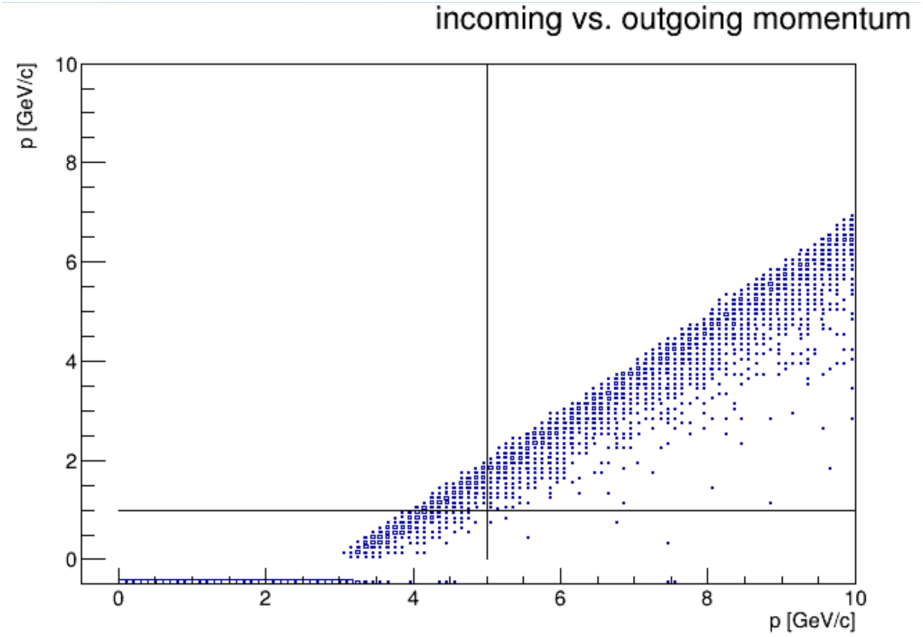

Figure 29: Outgoing (y axis) vs incoming (x axis) muon momentum on a 2.5 m iron block

12 Results

In this section we compare the reconstructed momentum distributions, p and p_T, between data and MC. The observed distributions are the result of physics processes responsible for the production of muons, through decays of pions and kaons, charm particles and also low mass resonances decaying to two muons and other rare processes, as well as the physics processes occurring while travelling through dense materials. We make no attempt to disentangle these effects. The main purpose is to validate our MC simulations for the muon background estimation for the SHiP experiment.

As discussed in previous section (see also Figure 12), the events outside the physical limits ($p >$ 350 GeV/c and $p_T >$ 5 GeV/c) are dominated by wrongly reconstructed trajectories due to background hits and the limited precision of the tracking detector. We restrict our comparison to 5 GeV/c $< p <$ 300 GeV/c and $p_T <$ 4 GeV/c. The lower limit of 5 GeV/c is an artefact of our MC simulation procedure. For momenta below 10 GeV/c, we only rely on the reconstruction with the tracking detector. Above 10 GeV/c we require the matching between the DT and RPC tracks.

Figure 30 and Figure 31 show the p and p_T distributions of muon tracks tagged with the RPCs. The distributions are normalized to the number of POT for data (see Section 5) and MC respectively. For the MC sample, muons from some individual sources are also shown in addition to their sum.

In Figure 32 we show the p_T distributions in slices of p. Table 5 shows a numerical comparison of the number of tracks in the different momentum bins.

Figure 33 gives a view of data and MC differences in the p/p_T plane. Printed are the

Table 5: Number of reconstructed tracks in different momentum bins per 10^9 POT per GeV/c for data and MC. The statistical errors for data are negligible. For data, the uncertainties are dominated by the POT normalization, 2.1%. For MC, the main uncertainty is due to a different reconstruction efficiency in MC compared to data, 3%.

Interval	data	MC	ratio
$5-10$ GeV/c	$(1.13 \pm 0.02) \times 10^5$	$(1.12 \pm 0.03) \times 10^5$	1.01 ± 0.04
$10-25$ GeV/c	$(2.40 \pm 0.05) \times 10^4$	$(1.68 \pm 0.05) \times 10^4$	1.43 ± 0.05
$25-50$ GeV/c	$(4.80 \pm 0.10) \times 10^3$	$(3.67 \pm 0.11) \times 10^3$	1.31 ± 0.05
$50-75$ GeV/c	$(9.83 \pm 0.2) \times 10^2$ ´	$(8.0 \pm 0.2) \times 10^2$	1.23 ± 0.05
$75-100$ GeV/c	$(2.95 \pm 0.06) \times 10^2$	$(2.5 \pm 0.08) \times 10^2$	1.20 ± 0.05
$100-125$ GeV/c	$(1.1 \pm 0.02) \times 10^2$	$(0.9 \pm 0.03) \times 10^2$	1.14 ± 0.05
$125-150$ GeV/c	21.0 ± 0.4	20.1 ± 7.5	1.04 ± 0.04
$150-200$ GeV/c	6.4 ± 0.1	6.6 ± 0.3	0.96 ± 0.04
$200-250$ GeV/c	0.76 ± 0.02	0.88 ± 0.06	0.86 ± 0.06
$250-300$ GeV/c	0.26 ± 0.01	0.26 ± 0.03	0.97 ± 0.11

ratios of data and MC tracks in bins of p and p_T. For momenta above 150 GeV/c, the MC underestimates tracks with larger p_T, while the total number of tracks predicted are in agreement within 20%.

The difference between data and MC could be reduced by increasing the contribution of muons from pion and kaon decays in the simulation.

Figure 34 shows the muon phase space distribution in data.

13 Conclusions

The physics processes underlying 400 GeV/c protons impinging on a heavy tungsten/molybdenum target are a convolution of the production of muons through decays of non-interacting pions and kaons, the production and decays of charm particles and low mass resonances, and the transportation of the muons through 2.4 m iron. Given the complexity of these processes, the agreement between the MC prediction and the measured rate is remarkable. This is good news for the SHiP estimates of backgrounds caused by muons. Some $20-40$% differences in the absolute rate are observed. The MC underestimates contributions to larger transverse momentum for higher muon momenta.

Systematic errors for the track reconstruction ((2 ± 3)% and POT normalization $(710 \pm 15$ POT$)/\mu$-event have been studied and estimated.

References

[1] The SHiP Collaboration, *A facility to Search for Hidden Particles (SHIP) at the CERN SPS*, April 2015, arXiv:1504.04956v1.

[2] The SHiP Collaboration, *Muon flux measurements for SHiP at H4*, CERN-SPSC-2017-020, June 2017.

[3] R. Zimmermann, J. Ebert, C. Hagner, B. Koppitz, V. Savelev, W. Schmidt-Parzefall, J. Sewing, Y. Zaitsev, *The precision tracker of the OPERA detector*, *Nucl. Instrum. Meth. A*, **555**, 435-450, (2005).

[4] D. Bick et al., *Alignment of the muon flux spectrometer in FairShip using the survey measurements*, CERN-SHiP-NOTE-2019-001, April 2019.

[5] M. Rosenthal et al., *Magnetic Field Measurements of the GOLIATH Magnet in EHN1*, CERN-ACC-NOTE-2018-0028, March 2018.

[6] P. Gorbunov, *DAQ Framework for the 2018 combined beam tests*, CERN-SHiP-INT-2017-004, November 2017.

[7] P. Gorbunov, *Trigger and DAQ conditions during the 2018 beam tests*, CERN-SHiP-INT-2019-004, October 2019.

[8] H. Dijkstra, *Normalization of proton flux during muon flux beam test*, CERN-SHiP-INT-2019-001, April 2019.

[9] W. Erni et al., *Technical design report for the $\overline{P}$ANDA (Anti$\underline{P}$roton $\underline{An}$nihilations at $\underline{Da}$rmstadt) Straw Tube Tracker*, Eur. Phys. J. A (2013) **49**: 25

[10] C. Höppner et al., *A novel generic framework for track fitting in complex detector systems*, *Nucl. Instrum. Meth. A*, **620**, Issue 2-3, 518-525, (2010).

[11] T.Sjöstrand, S. Mrenna and P. Skands, *A brief introduction to Pythia 8.1*, *Computer Physics Communications*, **178**(11), 852-867, 2008.

[12] S. Agostinelli et al., *GEANT4: A Simulation toolkit*, *Nucl. Instrum. Meth.*, **A506**, 250-303, (2003).

[13] H. Dijkstra, T. Ruf, *Heavy Flavour Cascade Production in a Beam Dump*, CERN-SHiP-NOTE-2015-009, December 2015.

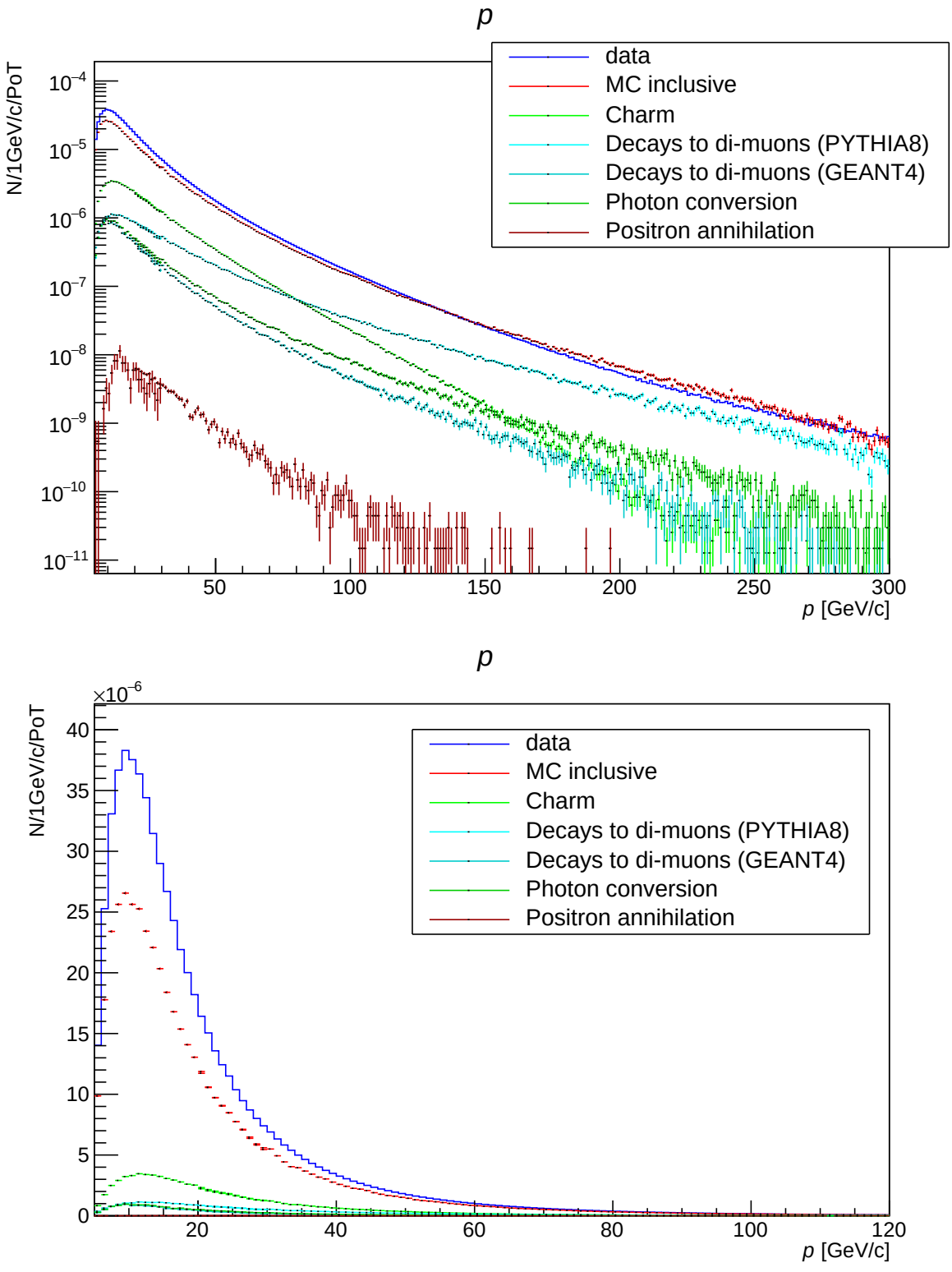

Figure 30: Momentum distributions from data and MC, top full range in log scale, bottom detail of the low momentum range with a linear scale. The distributions are normalized to the number of POT. For MC data, some individual sources are highlighted, muons from charm (green), from dimuon decays of low mass resonances in Pythia8 (cyan), in Geant4 (turquoise), photon conversion (dark green) and positron annihilation (brown).

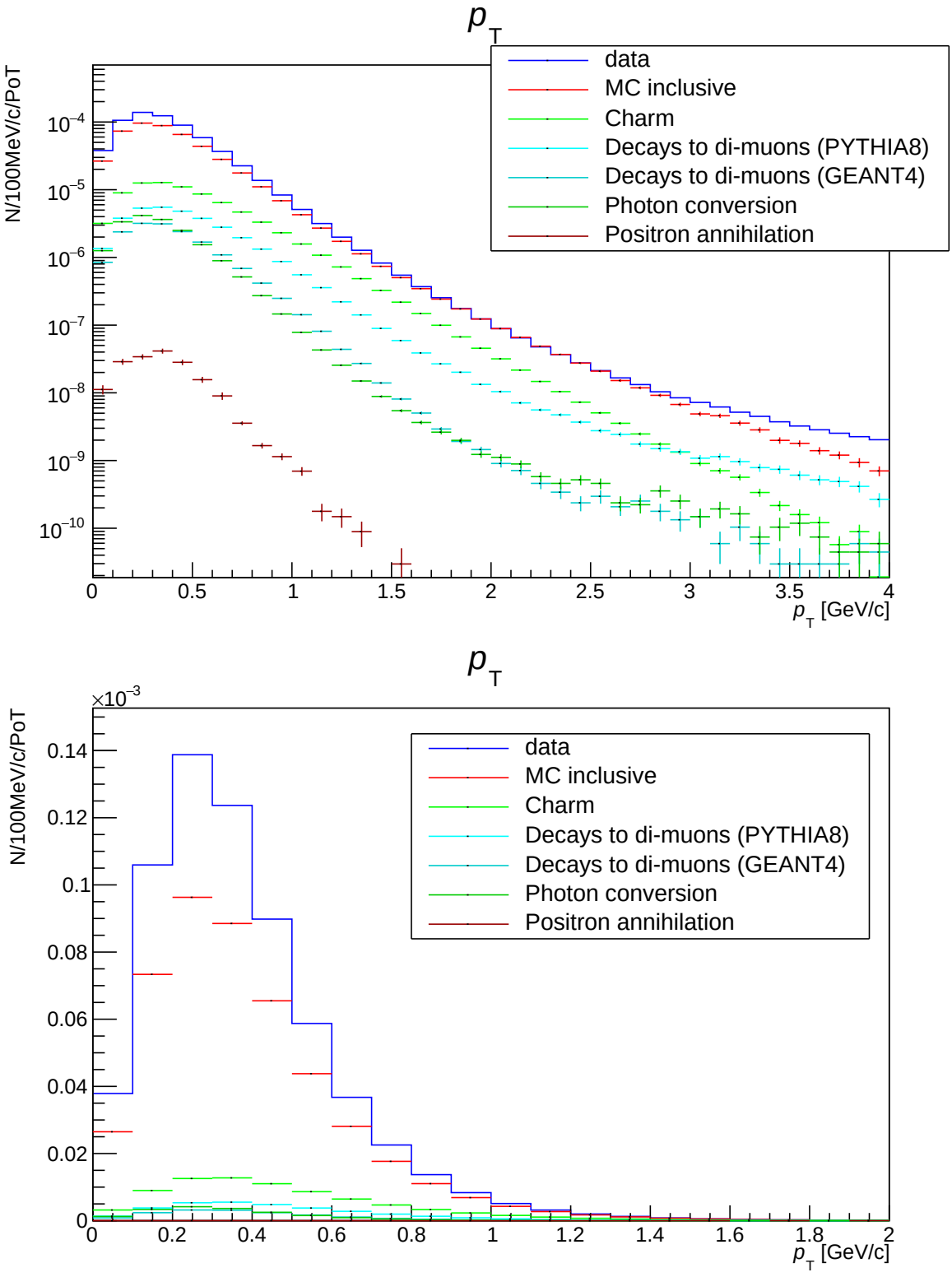

Figure 31: Transverse momentum distributions from data and MC, top full range in log scale, bottom detail of lower transverse momentum with a linear scale. The distributions are normalized to the number of POT. For MC data, some individual sources are highlighted, muons from charm (green), from dimuon decays of low mass resonances in Pythia8 (cyan), in Geant4 (turquoise), photon conversion (dark green) and positron annihilation (brown).

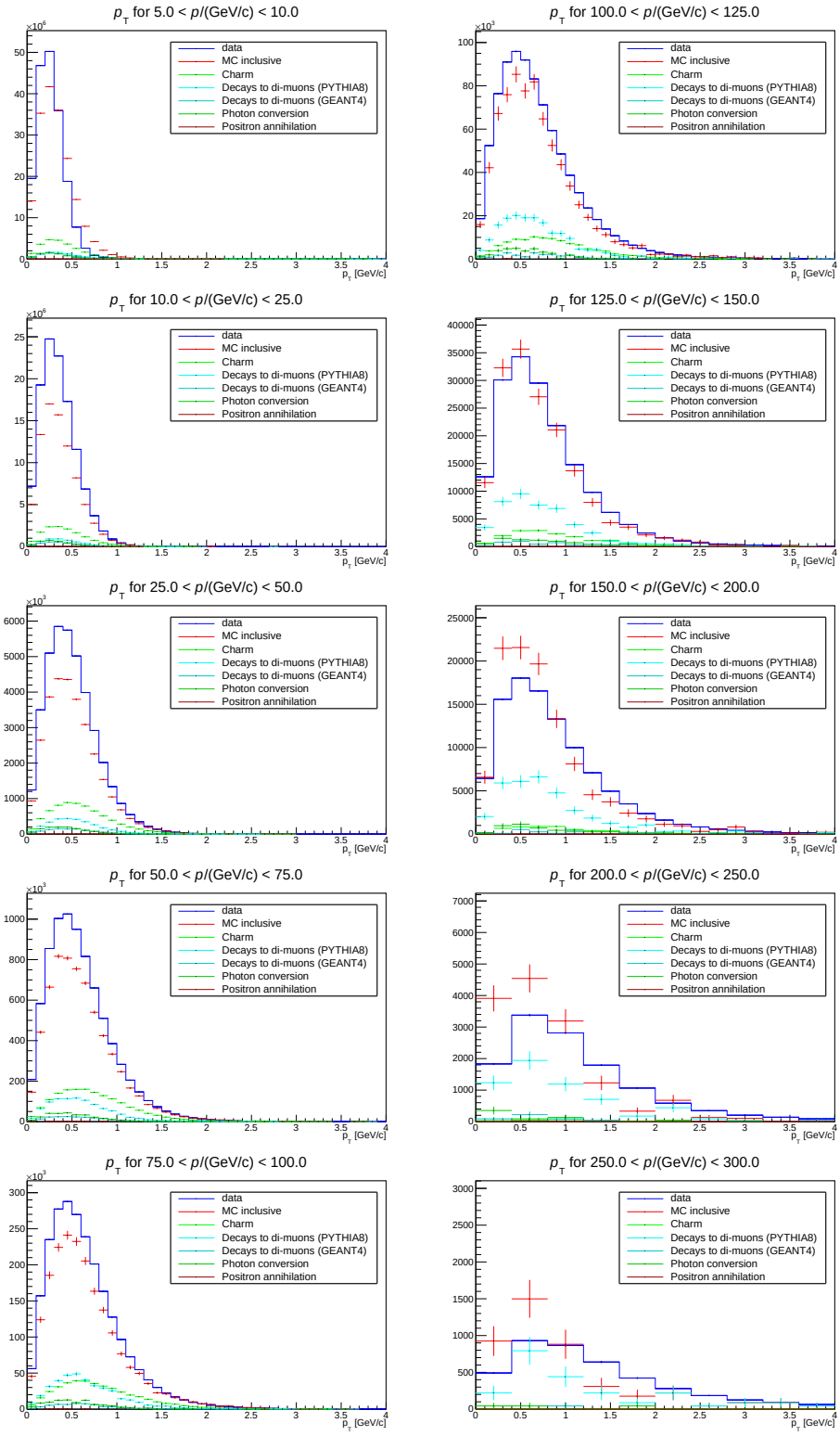

Figure 32: p_T distributions in slices of p for data and MC.

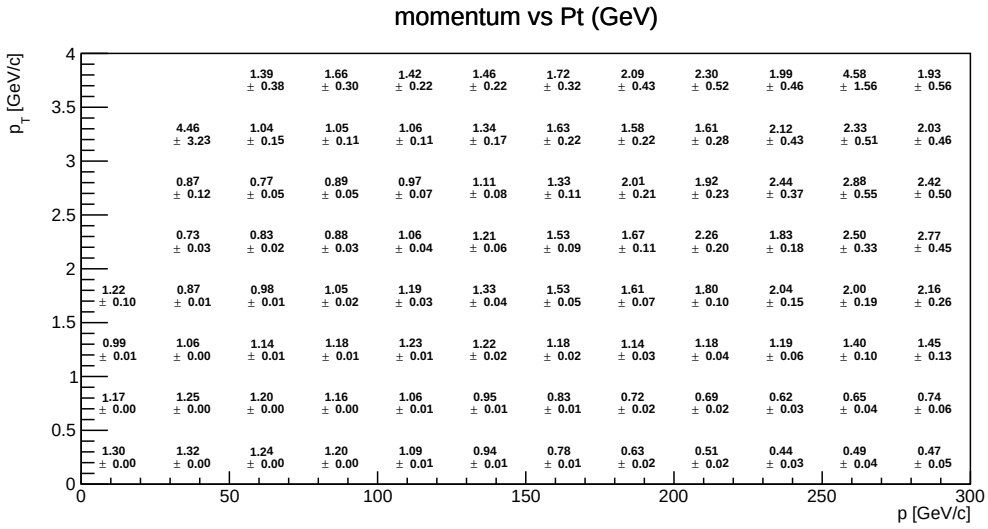

Figure 33: Ratio of data and MC tracks, $R = \frac{N_{data}}{N_{MC}}$ in bins of p and p_T.

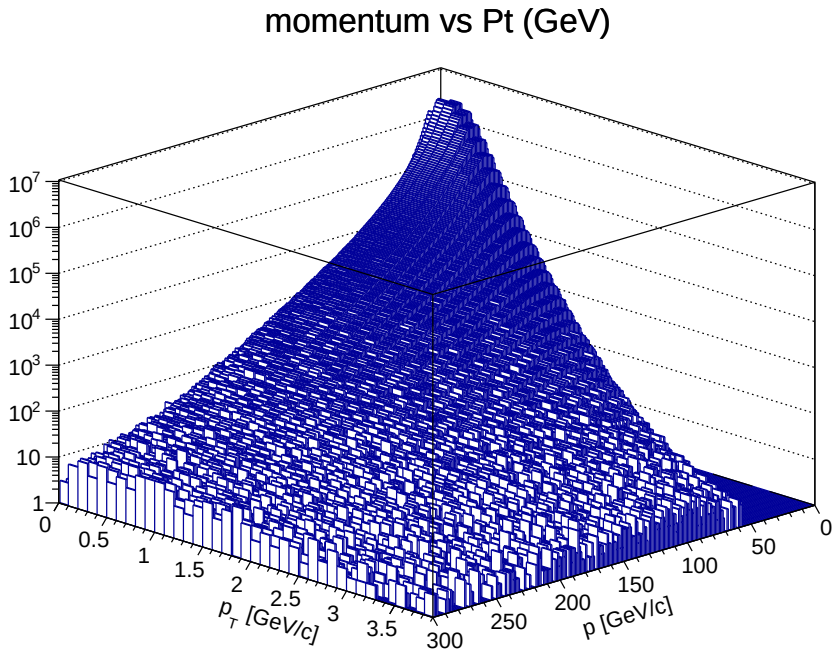

Figure 34: p_T vs p for data.